Carbon 167 (2020) 322–344

Contents lists available at ScienceDirect

Carbon

journal homepage: www.elsevier.com/locate/carbon

Review article

Carbon dots with red/near-infrared emissions and their intrinsic merits for biomedical applications

Hui Ding [a], Xuan-Xuan Zhou [a], Ji-Shi Wei [b], Xiao-Bing Li [a], Bo-Tao Qin [a], Xiao-Bo Chen [c], Huan-Ming Xiong [b, *]

[a] Key Laboratory of Coal Processing and Efficient Utilization of Ministry of Education and College of Chemical Engineering, China University of Mining and Technology, Xuzhou, 221116, Jiangsu, PR China
[b] Department of Chemistry and Shanghai Key Laboratory of Molecular Catalysis and Innovative Materials, Fudan University, Shanghai, 200433, PR China
[c] School of Engineering, RMIT University, Carlton, 3053, VIC, Australia

ARTICLE INFO

Article history:
Received 30 April 2020
Received in revised form
4 June 2020
Accepted 7 June 2020
Available online 12 June 2020

ABSTRACT

As a promising luminescent nanomaterial, carbon dots (CDs) have received tremendous attention for their great potential in biomedical applications, owing to their distinctive merits of ease in preparation, superior optical properties, good biocompatibility, and adjustable modification in structure and functionalities. However, most of the reported CDs exhibit insufficient excitation and emission in red/near-infrared (R/NIR) regions, which significantly limits their practical applications in biomedical assays and therapy. In the latest years, extensive studies have been performed to produce CDs with intensified R/NIR excitation and emission by designed reactions and precise separations. This review article summarizes state-of-the-art progress towards design and manufacture of CDs with long-wavelength or multicolor emissions, involving their synthetic routes, precursors, and luminescence mechanisms. Meanwhile, the applicable availability of CDs in bioimaging, sensing, drug delivery/release, and photothermal/photodynamic therapy, is systematically overlooked. The current challenges concerning feasible controls over optical properties of CDs and their new opportunities in biomedical fields are discussed.

Contents

* Corresponding author.
E-mail address: hmxiong@fudan.edu.cn (H.-M. Xiong).

https://doi.org/10.1016/j.carbon.2020.06.024
0008-6223/

1. Introduction

Over the past decade, carbon dots (CDs), an emerging class of luminescent carbon-based nanomaterials, have attracted great attention from multiple disciplines owing to their superior properties and widespread applications [1–4]. CDs are usually defined as a group of small sized carbon nanostrcutures with a diameter below 10 nm, including graphene quantum dots (GQDs), carbon quantum dots (CQDs), carbon nanodots (CNDs), and carbonized polymer dots (CPDs). CDs can be readily produced from various carbon sources with two kinds of synthetic approaches, namely "top-down" and "bottom-up" [5–8]. The former method involves cutting down large carbon materials into fine nanoparticles, while the latter refers to the preparation of CDs by chemically fusing organic molecules through dehydration and carbonization under hydrothermal/solvothermal/thermal conditions [9–11]. Typically, obtained CDs possess a graphite core and an amorphous shell consisting of numerous surface functionalities, such as carboxyl, hydroxyl, amide, and carbonyl moieties [12–14]. Those unique structures and components endow CDs remarkable properties, such as high water solubility, tunable luminescence emission, great biocompatibility, low toxicity, excellent photostability, easy bioconjugation and high specific surface area, which consequently inspires a great potential for applications in bioimaging, biosensing, drug delivery, and cancer diagnosis and therapy, etc. [15–17]. However, most of the reported CDs exhibit strong absorptions in the UV range and visible photoluminescence (PL) emissions less than 600 nm, which gives rise to strong tissue absorption, shallow tissue penetration, high interference from auto-fluorescence, and severe photodamage to tissues and cells and thus greatly limits their further applications [18–20]. Therefore, it is of significant importance to synthesizing intensive red/near-infrared emitting CDs (R/NIR-CDs) under long-wavelength excitation, thereby making them appropriate substitutes for typical semiconductor quantum dot (QDs) and organic dyes in biomedical applications.

In recent years, numerous efforts have been made to improve the absorption and emission intensity of CDs in the R/NIR windows, and apply them in various biotechnologies [21]. In the case that the PL mechanism remains unclear, a certain number of highly fluorescent CDs with long-wavelength emissions have been produced through choosing proper C sources or reaction media, altering reaction conditions, or performing post-treatment such as surface passivation and separation [22–24]. The obtained CDs in that way possess the highest quantum yield (QY) of 86% in red light range, and show a great potential for optical-related services [25]. In addition, much attention has also been focused on understanding the origins of luminescent features of CDs with long-wavelength or multicolor emissions [26,27], which is assumed as key to underpin PL related mechanisms, and thus to guide rational design towards CDs with desired optical properties. Both experimental and theoretical studies confirm that evident PL redshifts can be triggered by means of increasing particle size, engineering surface state, and improving heteroatom doping, individually or synergistically [9,28]. A few research groups realized both the efficient absorption and emission of CDs in NIR regions (with a wavelength larger than 650 nm). However, such NIR-CDs remain suffering poor water solubility, low absorption and emission efficiency, and broad full width at half maximum (FWHM), which is detrimental to the expected performances in biomedical services [29]. To date, a few review articles in open domain have covered the synthetic strategies of highly fluorescent CDs and their applications for biomedical, optoelectronic, photocatalytic and energy storage aspects [13,18,30–32], but cast little attention on synthesis, PL modulation, and biomedical feasibility of CDs with R/NIR or multicolor emissions, in particular the sound techniques for redshifting emission wavelengths and regulating FWHM.

This review attempts to summarize the state-of-the-art advances in the development of CDs with R/NIR or multicolor emissions. Key factors in synthesizing CDs with such optical properties, involving synthesis strategies, precursors, reaction conditions, and separation techniques will be reviewed in the first part, followed by discussion of PL mechanisms of CDs with long wavelength or multicolor emissions. Secondly, the approaches to decrease FWHM of CDs and their luminescence mechanisms are highlighted. Thirdly, recent progress on the applications of R/NIR-CDs in bioimaging, sensing, drug delivery/release, and photothermal/photodynamic therapy is outlined. Finally, the potential development and challenges in terms of preparation and application of R/NIR-CDs in the future are provided.

2. Synthesis of CDs with R/NIR or multicolor emissions

Due to a lack of understanding about how a structure of CDs contributes to their luminescence, it remains a great challenge to fine-tune the emission wavelengths of the final CD products toward long-wavelength region. Nonetheless, materials scientists still made great efforts to produce highly efficient CDs with absorption and emission both in red/NIR regions via screening precursors, optimizing reaction conditions, or purifying CD mixtures [33–35]. Among them, the selection of carbon precursors is of crucial importance because they have a significant influence on structure and functional components of CDs, such as particle size, graphitization degree, element content, and surface functional groups, and so on, which in turn determines optical properties of the final

products [36–38]. So far, a large number of CDs with R/NIR or multicolor emissions have been reported [21], which were stemmed from precursors containing unique structures or components. Doping CDs with heteroatoms could introduce new energy levels, whilst introduction of aromatic structure into CDs could inherently reduce energy gaps through generating large sp^2 domains. Both those approaches are beneficial to the tuning of absorption and emission of CDs towards long-wavelength region. As a result, various precursors, ranging from bulk carbon materials to small organic molecules, aromatic compounds, and even biomass, are reported for synthesizing CDs with R/NIR or multicolor emissions.

2.1. Bulk carbon materials

In general, bulk carbon materials are non-luminent. Fluorescence emissions is only possible in nanosized carbon based materials. In the early studies, many kinds of larger carbon materials, such as graphite, carbon fibers, tire soot, carbon nanotubes, graphene oxide and coal, have been treated by acid oxidation, electrochemical etching, or laser ablation for yielding short-wavelength emissive CDs with high QYs, which however are not suitable for biomedical applications [39–41]. With further development, some bulk carbon materials are used as precursor for producing CDs with long-wavelength or tunable emissions. In 2013, Kim's group reported preparation and isolation of fluorescent CDs from an environmental pollute, i.e. tire soot, by means of oxidative nitric acid treatment [42]. The broad emission spectra of the obtained CDs span from 430 to 710 nm with a strong dependence on the excitation wavelength. Importantly, comparable NIR fluorescence intensity of CDs was acquired even at excitation wavelength greater than 640 nm. Therewith, Tan et al. reported a simple electrochemical exfoliation strategy for preparing water-soluble, small sized, red fluorescent CDs from graphite precursor in $K_2S_2O_8$ solution [43]. PL spectra of the CDs show an excitation-independent emission at 610 nm, which is attributed to their larger sp^2 clusters in carbon cores, as shown in Fig. 1a and b.

In addition to long-wavelength emission, PL tunable CDs were also produced from bulk carbon materials with similar methods. For example, through chemical oxidation treatment of carbon fibers in nitric acid solution followed by ultrafiltration, Bao and coworkers prepared a series of water soluble CDs with tunable PL emission from blue to red and QYs within 1.8–20.7% (Fig. 1c) [44]. The tunable emission and relatively low QY indicate that the photoluminescence of CDs is derived from the defect state emission. Tseng's group synthesized blue-, green-, yellow-, and red-emitting GQDs through heteroatom doping and hydroxyl-radical-induced decomposition of graphene oxide (Fig. 1d–f) [45]. The obtained GQDs are comprised of a single or a few layered graphene sheets with abundant oxygen- and nitrogen-related functional groups attached to the edges, exhibiting abroad absorption across the entire visible region, excitation-independent emissions, moderate quantum yields (1–10%), and nanosecond fluorescence lifetimes. Therewith, Hu et al. presented a simple and energy-efficient approach for large scale synthesis of CDs using coal pitch as carbon source and a blended solution of formic acid and H_2O_2 as oxidation agent (Fig. 1g) [46]. Interestingly, the obtained CDs exhibited concentration-dependent morphologies in aqueous solutions, and then gave rise to tunable PL emission across the entire visible light spectrum (Fig. 1h). Although top-down routes are feasible for mass production of CDs given the moderate operating conditions, the prepared CDs are usually with low QYs particularly in the long wavelength region, which may be ascribed to their surface-state emission nature.

2.2. Small organic molecules

Differing from larger carbon materials, small organic molecules are amorphous, consisting of a large number of polar functional groups containing various heteroatoms. They are sound precusors for preparation of CDs through bottom-up techniques, such as combustion/thermal treatments, supported synthetic and microwave synthetic methods [47]. Elevated reaction temperatures associated with typical bottom-up operations trigger a series of complex reactions to organic precursors, i.e. dehydration, polymerization, and carbonization, which finally leads to the formation of carbon nanoparticles that exhibit structures and components close to those of the precursors [4]. Although numerous small organic molecules have been developed to synthesize CDs so far, most of them emit blue or green color under UV irradiation, which are not desired for biomedical applications. It is noted that a few CDs with R/NIR or multicolor emissions were prepared out of small organic molecules with specific functional groups, such as citric acid (CA), amino acid, and saccharides, etc.

CA possesses a few oxygen-containing functional groups, and easily reacts with organic molecules containing an amino group, to form nitrogen-related species under supercritical conditions, which exist in carbon cores or on CD surfaces in the form of amino, amidic, pyridinic, pyrrolic, etc. [48–50]. The increment in the dehydration reaction between CA and amino group and carbonization degree leads to increasing particle size of and nitrogen content in CDs, which facilitates a reduction in band gap between the highest occupied molecular orbital (HOMO) and the lowest unoccupied molecular orbital (LUMO), thereby causing a pronounced red shift in absorption and emission spectra of CDs [51]. Thus, CDs with R/NIR or multicolor emissions can be produced using a mixture of CA and organic molecules with different amine groups as precursors. In Fig. 2a–d, Lin's group first reported truly fluorescent excitation-dependent CDs across a wide range from 330 to 600 nm through microwave-assisted treatment of CA and formamide at 160 °C for 1 h [52]. They demonstrated that further amidation reactions between CA and formamide and carbonization could occur upon raising reaction temperature and prolonging reaction time, consequently resulting in more C=C, C=N/C=O, and C-N bonds within CDs, which are responsible for their long-wavelength emissions. Through heating a formamide solution of CA and ethylenediamine (EDA) in an autoclave followed by precipitation with acetone, our group also produced highly fluorescent R-CDs with a QY of up to 53% on a large scale (Fig. 2e) [53]. These R-CDs possessed a remarkably increased number of nitrogen- and oxygen-related functional groups and nitrogen-derived structures due to a higher degree of dehydration and carbonization of precursors, which synergistically contributes to the intensive red emission. One year later, using CA and urea as carbon source and N, N-dimethylformamide (DMF) as reaction medium, Sun's group synthesized CDs playing multiple-color emission across the entire light spectrum through regulating thermal-pyrolysis temperature and ratio of reactants [54], as shown in Fig. 2f and g. Emissions were shifted from blue to red region as a result of increasing effective conjugation length and quantity of COOH. Very recently, using CA and amino-containing polyethyleneimine (PEI) as C precursors and formamide as reaction solvent, Lin's group reported amino-rich R-CDs with a PL peak centered at 640 nm [55], which also exhibit possess a superior photothermal (PT) conversion efficiency of 46% under 671 nm NIR laser.

In addition to the aforementioned small organic molecules, CA can react with some benzene ring-containing compounds to produce CDs with R/NIR or multicolor emissions, such as p-aminosalicylic, 1,5-diaminonaphthaleneaphen, 8-hydroxyjulolidine, and neutral red, etc [15]. In 2017, Yang's group synthesized orange-red

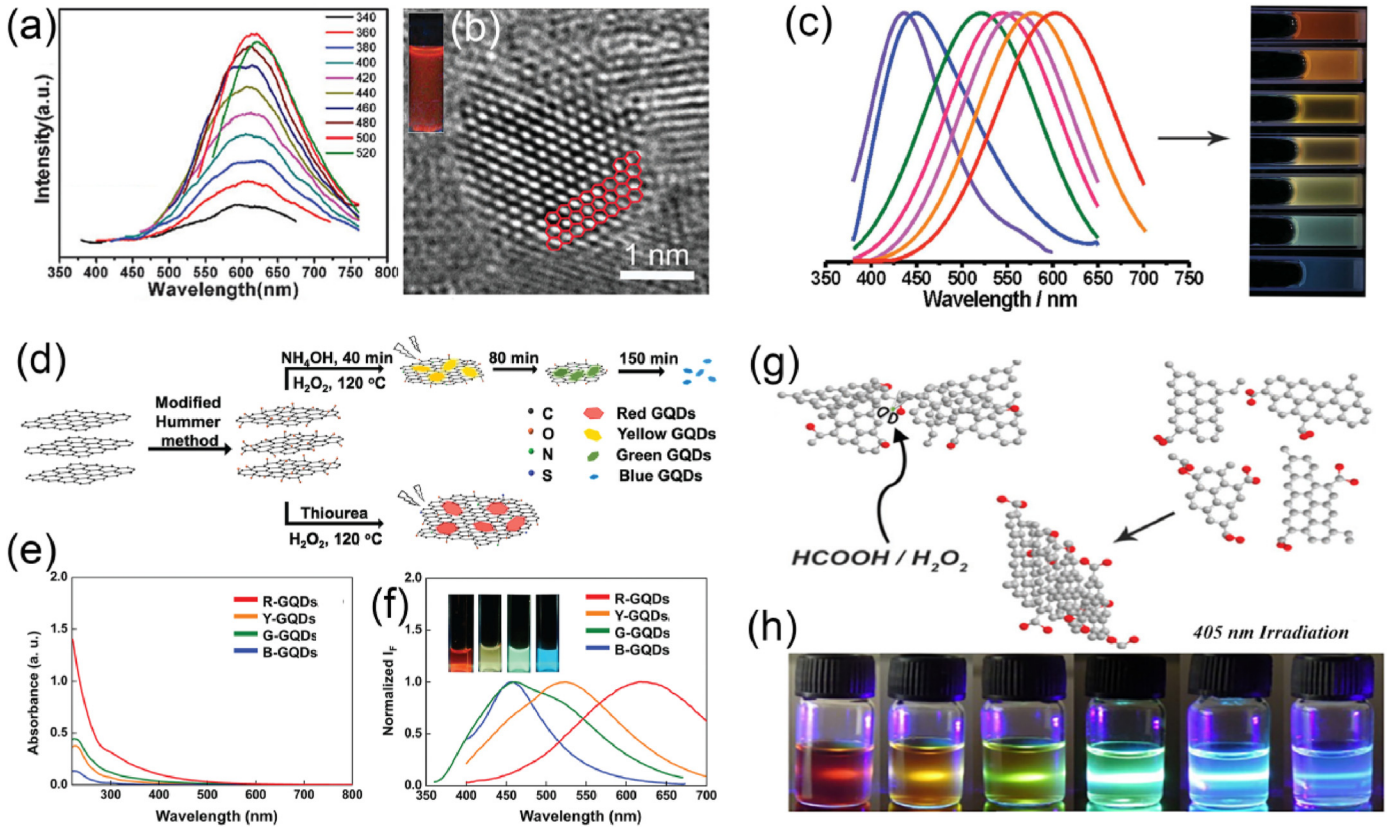

Fig. 1. (a) PL spectra and (b) HRTEM image of R-CDs. The inset is a photograph of a R-CD solution under 365 nm illumination. (c) Normalized PL spectra (left) of as-prepared multicolor CDs and their corresponding optical images (right) with excitation at 360 nm. (d) Preparation illustration, (e) UV–vis absorption spectra, and (f) Normalized PL spectra of fluorescent R-GQDs, Y-GQDs, G-GQDs, and B-GQDs through hydroxyl radical-induced decomposition of GO. Inset: photographs of obtained multicolored GQD solutions under UV light. (g) Schematic illustration of the preparation procedures of multicolored CDs by treating coal pitch with a mixture of formic acid and H_2O_2. (h) Photographs of CDs solutions with different concentrations under UV lamp. Reprinted and adopted with permission from Ref. [43–46]. (Copyright 2015 and 2017 Royal Society of Chemistry and Copyright 2015 and 2016 Wiley and Sons.). (A colour version of this figure can be viewed online.)

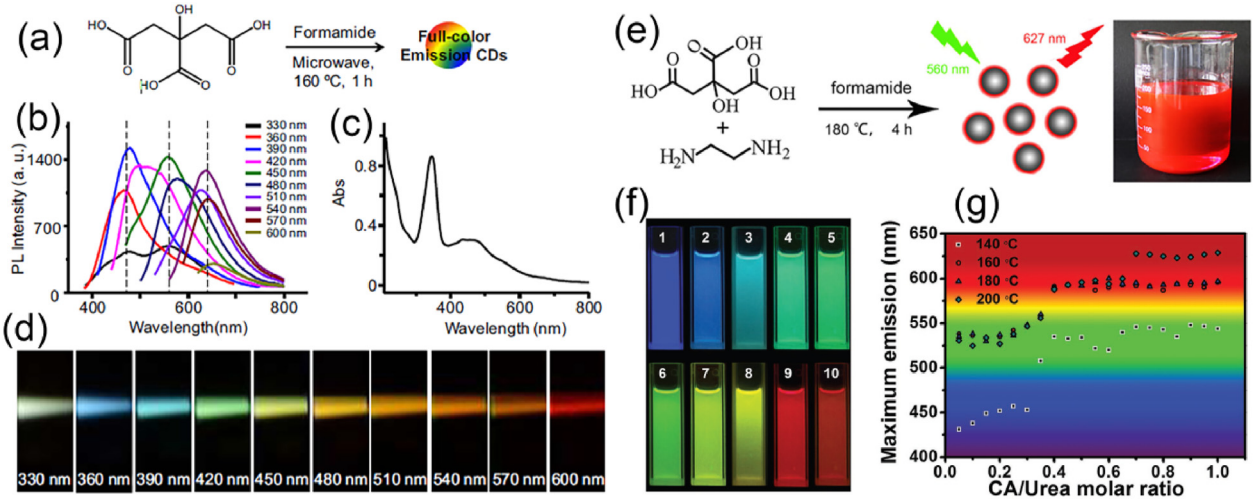

Fig. 2. (a) Schematic illustration of preparation, (b) FL spectra, and (c) UV–vis absorption spectra of the full-color emission CDs; (d) FL emission photographs of the obtained full-color emission CDs recorded from 330 to 600 nm in 30 nm increments. (e) Synthetic route of R-CDs and products under sunlight. (f) Optical images of luminescence CDs prepared from different reaction conditions under different excitation light; (g) the maximum emission peaks of CDs at different molar ratios of CA to urea and different reaction temperatures. Reprinted and adopted with permission from Refs. [52,53and55]. (Copyright 2015 and 2018 Wiley and Sons and Copyright 2017 American Chemical Society.). (A colour version of this figure can be viewed online.)

emission solid-state CDs through hydrothermally treating an acid solution of CA and p-aminosalicylic acid (Fig. 3a) [56]. In comparison with its aqueous solution, solid state CDs exhibited a remarkable PL redshift owning to supramolecular crossing-linking

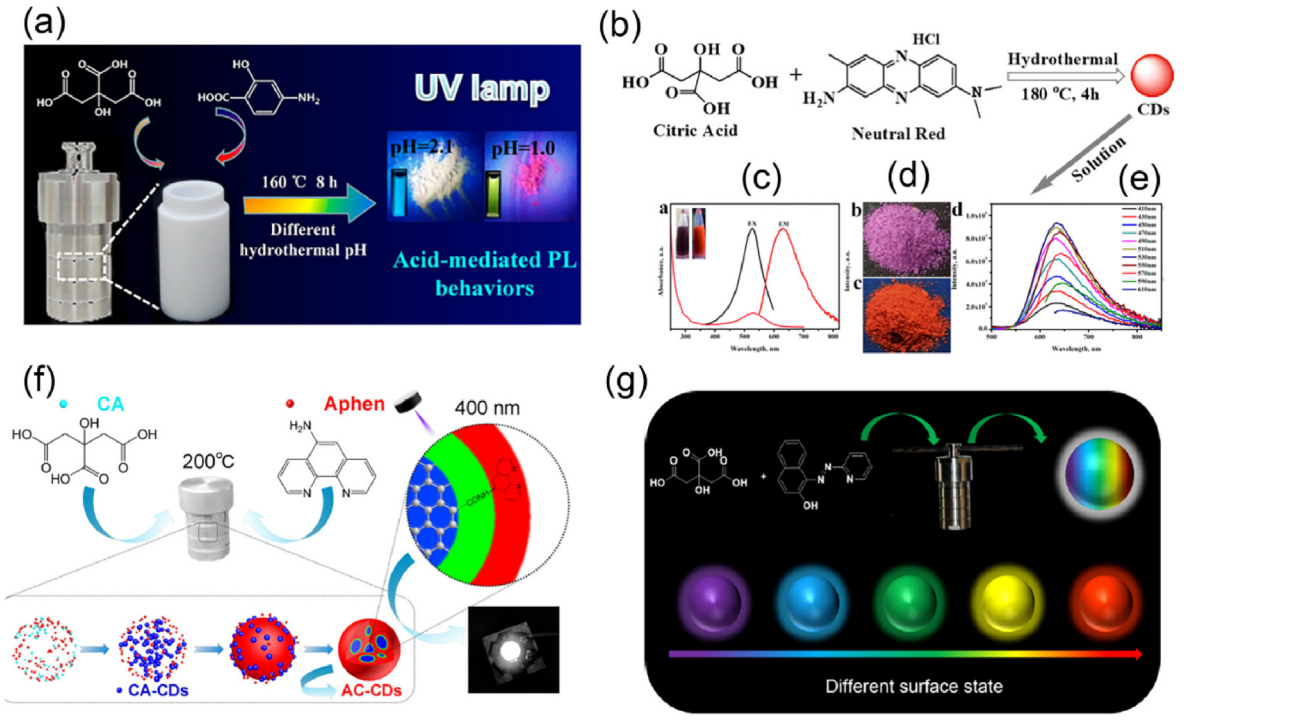

Fig. 3. (a) Schematic illustration of the preparation of orange-red emission solid-state CDs. Inset: photographs of liquid state and solid state CDs synthesized with different pH values. (b) Synthetic route, (c) UV–vis absorption, fluorescence excitation, and (e) emission spectra of R-CDs in aqueous solution; (d) photographs of R-CD solid powder under daylight and 365 nm UV light. (f) Schematic illustration of preparation and application of multiple-core@shell-structured CDs. (g) Schematic diagram of synthesis process of CDs. Reprinted and adopted with permission from Ref. [57–60]. (Copyright 2017, 2017 and 2018 American Chemical Society and Copyright 2019 Springer.). (A colour version of this figure can be viewed online.)

between adjacent CD particles, which indicates their potential for solid-state light emitting diodes (LED) applications. In the same year, using CA and neutral red as raw materials and ultrapure water as solvent, Peng's group reported the fluorescent CDs with red emission both in aqueous solution and solid state (Fig. 3b–e) [57]. The obtained CDs showed a QY of 12% in water, good photostability at UV irradiation, low toxicity, and could finally be used as promising bioimaging and biosensing of noble metal ions in PC12 cells and zebrafish. One year later, Zhang et al. constructed nitrogen-doped multiple-core@shell-structured CDs with controllable fluorescence via one-pot hydrothermal method from CA and 5-amino-1,10-phenanthroline as reactants (Fig. 3f) [58]. The special structure could endow CDs with tricolor emissions of blue at 430 nm, green at 500 nm, and red at 630 nm. Importantly, the maximum PL QY of CDs in the red light region reaches up to 67% by increasing their solution concentration, which indicates the occurrence of fluorescence resonance energy transfer (FRET) process between CDs. Very recently, Yan and coworkers synthesized a type of multicolor emissive CDs by solvothermal treatment of CA and 1-(2-pyridylazo)-2-naphthol (PAN) in ethanol (Fig. 3g) [59]. By adjusting the concentration, the fluorescence spectra of CDs in organic solvents can be tuned from 350 to 750 nm, as a result of self-absorption and energy transfer between the multiple energy levels upon aggregation of multicomponent in CDs at high concentrations.

Amino acids, a basic unit of proteins, are one of the important compounds to the human beings, and have been used as an ideal carbon source for producing CDs with R/NIR or multicolor emissions. For example, Pan et al. synthesized NIR-CDs emitting at 683 nm through microwave-assisted heating of a formamide solution of glutathione (Fig. 4a–c) [60]. These obtained NIR-CDs are water soluble, exhibiting a QY of 17% under excitation of 850 nm fs (fs) pulse laser. Further studies revealed that the excitation-independent emission of N-CDs derives predominantly from the surface molecular state mechanism. Thereafter, by employing different ratios between arginine, EDA, naphthalene dianhydride, and 2, 6-dibromonaphtalene, dianhydride, Maurizio's group tuned emission color of CDs from blue to red [61], resulting in pure white-light emission covering a broad range from 400 to 700 nm (Fig. 4d and e). In this regard, using L-glutamic acid and o-phenylenediamine as reactants, our group reported a series of excitation-independent luminescent CDs with high QYs (13–54%) across the entire visible spectrum (443–745 nm) via a novel solvent-controlled synthetic route (Fig. 4f) [62]. The distinct optical properties of resultant CDs are based on their differences in the particle size, and the content of graphitic nitrogen and oxygen-containing functional groups, which can be modulated by controlling the dehydration and carbonization processes. In 2019, Xu's group prepared red/orange dual-emission CDs using L-cystine, o-phenylenediamine, and ethanol as raw ingredients via a solvothermal route [63]. The dual-emission CDs showed an excitation-independent PL behavior, and relatively high PL QY of 35.7% towards near-infrared fluorescent peak up to 648 nm. With the advancement of characterization techniques, N, S-dopants were found to not only enrich electronic states, but also lead to the creation of in-gap trap states that could act as nonradiative and recombination centers, thereby resulting in the strong red emission.

Saccharides are a main energy source required by all living creatures to maintain life activities, which have also been adopted as raw materials [15]. In 2013, Jana's group reported gram-scale synthesis of highly fluorescent CDs with tunable visible emission

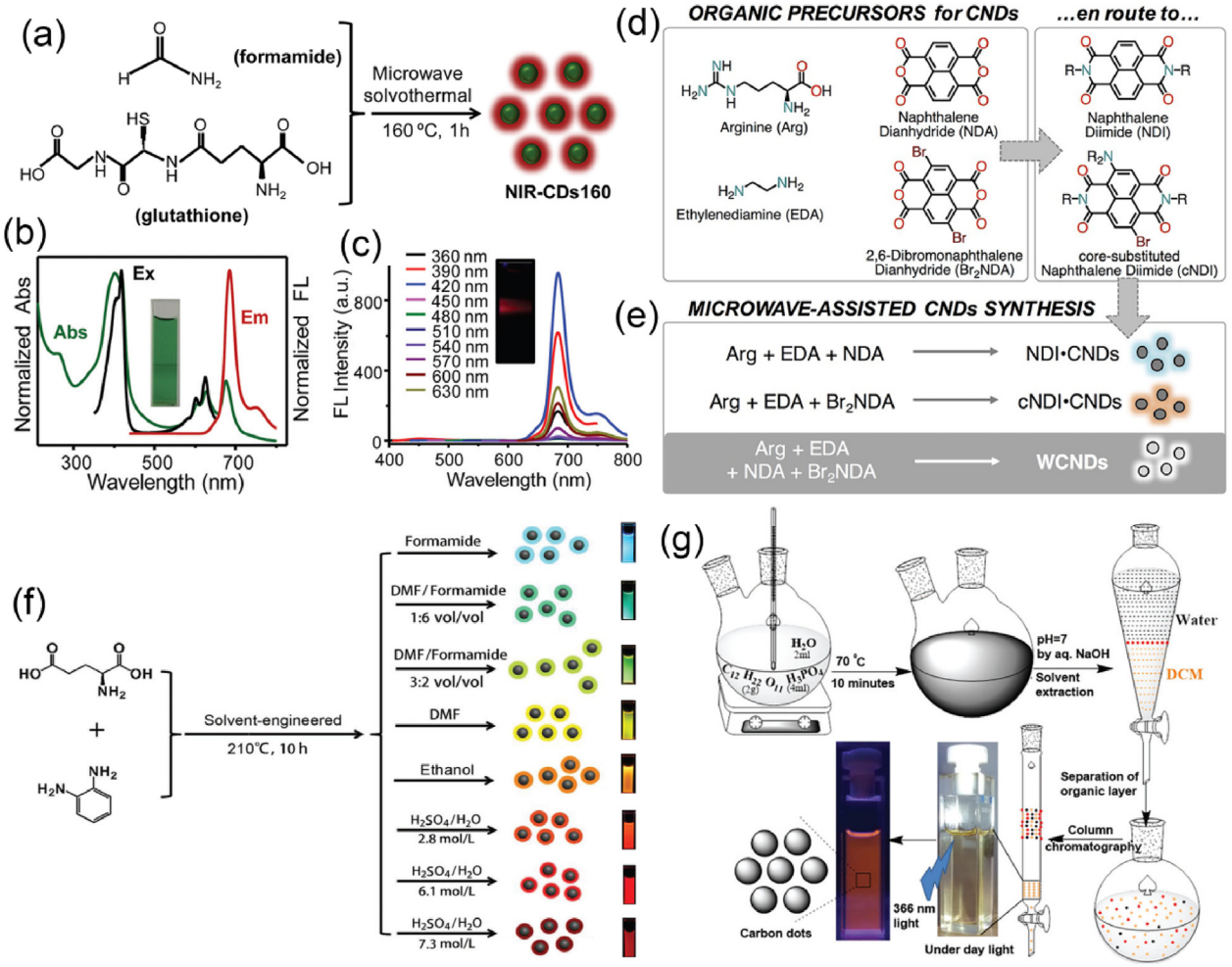

Fig. 4. (a) Schematic illustration of preparation, (b) UV–vis absorption, fluorescence excitation, and (c) emission spectra of NIR-CDs. Inset: photographs of NIR-CD aqueous solution under daylight and UV light. (d) Molecular structures of the organic precursors and (e) microwave-assisted synthesis starting from the depicted organic precursors. (f) A solvent-engineered strategy for synthesis of multicolor fluorescent CDs using l-glutamic acid and *o*-phenylenediamine as starting materials. Inset: photos of the as-prepared CDs and UV light. (g) Preparation and purification of orange-red emitting CDs using sucrose and H_3PO_4. Reprinted and adopted with permission from Ref. [61-63and67]. (Copyright 2016 and 2016 Royal Society of Chemistry and Copyright 2017 and 2018 Wiley and Sons.). (A colour version of this figure can be viewed online.)

from blue to red through heating a series of carbohydrate at appropriate temperatures [64]. These resulting multicolored CDs showed pH-dependent PL emission, and relatively high QYs between 6 and 30%, which are correlated with their particle size and chemical composition. Three years later, through functionalizing already-prepared CDs with glucose, the same group reported the synthesis of R-CDs with high colloidal stability, 3% efficient PL QY and stable luminescence under continuous light exposure, which exhibited promising application in cell imaging [65]. Thereafter, Gude et al. produced orange-red emitting CDs from cost-effective and non-toxic saccharides, such as sucrose, fructose and glucose with regular laboratory equipment (Fig. 4g) [66]. Optical properties of those CDs are quite unique, exhibiting an excitation-independent PL emission, single exponential PL decay, and a significant stokes shift by 150 nm, which are associated with the only one type of chromophore hydroxymethylfurfural (HMF) derivative present within CDs. Apart from the above mentioned three kinds of small organic molecules, there are also few other aliphatic compounds that could be mixed with some amino-containing organic molecules to produce CDs with such optical properties, including maleic acid, glycol, tris, oxalic acid, and L-proline, etc [67–71].

2.3. Aromatic compounds

Aromatic compounds are a kind of prevalent precursors for producing CDs with R/NIR or multicolor emissions, especially those that are substituted with polar functional groups such as amino, hydroxyl, or sulfydryl [72]. It is ascribed to the fact that a suitable aromatic structure existing in precursors would inherently lower the energy gaps of CDs by generating large sp^2 domains through dehydration and carbonization reaction [73–75]. As a result, aromatic compounds could be used as a single precursor, or mixed with other organic molecules to produce CDs with long-wavelength emissions. In this section, we mainly discuss the employment of individual aromatic compounds or mixtures with other benzene ring-containing molecules except for aliphatic ones, which have been discussed in the previous section.

Aromatic amines that are composed of benzene rings and amino groups are an important class of raw materials for producing CDs with long-wavelength or multicolor emissions. Since the first report regarding the preparation of R-CDs from p-phenylenediamine (p-PDA) in 2015 [76], numerous long-wavelength or multicolor emission CDs were yielded with using aromatic amines as precursors. For instance, through heating treatment of o-

phenylenediamine (o-PDA) in HNO_3 aqueous solution (Fig. 5a), Yang's group reported excitation-independent R-CDs with optimal emission at 630 nm and a high QY of 32% [77]. Further studies indicate that such intensive red fluorescence is ascribed to the efficient conjugated aromatic π systems and hydrogen bonds of R-CDs. In 2019, as shown in Fig. 5b, employing N,N-dimethyl-, N,N-diethyl-, and N,N-dipropyl-p-PDA as raw materials, Fan's group synthesized three kinds of respective R-CDs emitting at 637, 642, and 645 nm, with the highest QY up to 86% in ethanol (Fig. 5c) [25]. Experimental characterization and theoretical investigations confirm that the red bandgap emission originates from a rigid π-conjugated skeleton structure, and a -NR_2 passivation plays a key role in inducing charge transfer excited state in the π-conjugated structure to afford high QY. In the same year, Liu's group prepared 25% efficient R-CDs from p-PDA, o-PDA, and dopamine by a one-pot hydrothermal method [78]. Those CDs possessed a variety of superior properties of high selectivity, excellent photostability, and low cytotoxicity, along with pH-sensitive linear responses over a range of 3.5–6.5, and thus were successfully applied to sense and visualize pH fluctuations in cells, tissue, and zebrafish.

Phenols are a type of aromatic compounds in which hydrogen atoms in benzene ring are substituted by hydroxyl groups and are also one of the most common ingredients to produce CDs with R/NIR or multicolor emissions. In 2018, through solvothermal treatments of three-fold symmetric phloroglucinol in ethanol followed by purifying by means of silica column chromatography, Yang's group achieved good stability, high color-purity, and multicolored emission triangular CDs with a QY up to 54–72%, which enables their applications in LEDs for the development of next-generation display technology [79]. Thereafter, as shown in Fig. 5d and e, Ghosh and coworkers reported the synthesis of R-CDs peaking at 600 nm with a QY of 25% in water [80], which involves controlled carbonization of resorcinol in ethylene glycol-Na_3PO_4 under air exposure. Interestingly, the method yielded 50–60 mg of R-CD samples in one batch without any chromatographic purification or dialysis, and thus could be easily adapted for a larger scale synthesis. Very recently, by heating 4-aminophenol in an ethanol solution at 195 °C for 1 h in autoclave, Fan's group synthesized water-soluble, uniform-sized R-CDs emitting at 620 nm with an absolute QY of 20% [81]. Those R-CDs were stable after three-month storage and 24 h of UV irradiation, respectively, demonstrating superior optical properties.

Polythiophene derivatives consisting of aromatic monomers, are increasingly used in the synthesis of with R/NIR or multicolor emissions. In 2014, Ge and coworkers reported the first example of producing R-CDs using polythiophene derivatives as raw materials [82]. In that work, they firstly designed precursor molecules, polythiophene derivatives (PT2), then hydrothermally heated them,

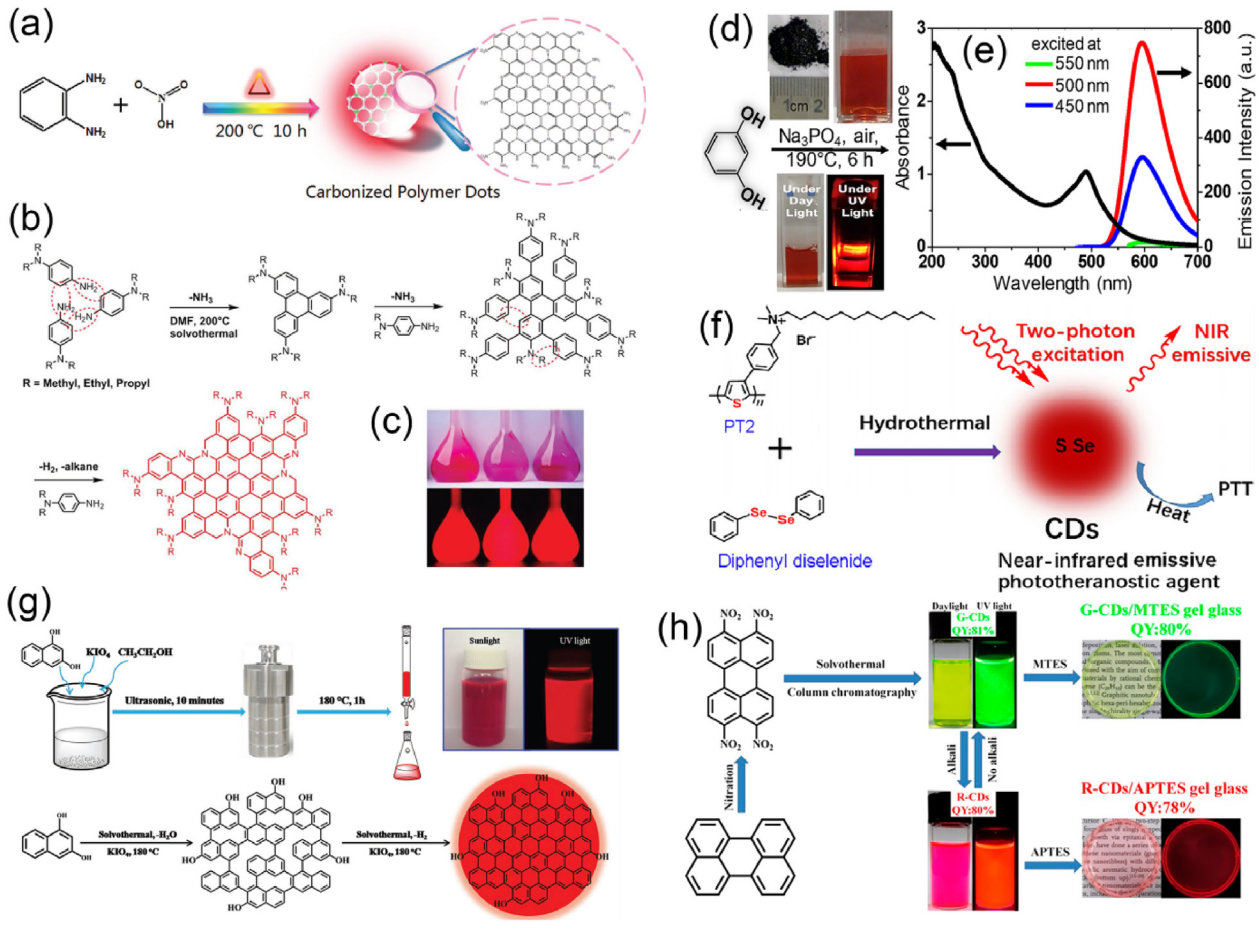

Fig. 5. (a) A preparation illustration of R-CDs from p-phenylenediamine. (b) Synthesis of R-CDs by solvothermal treatment of *N*,*N*-dimethyl-, *N*,*N*-diethyl-, and *N*,*N*-dipropyl-p-PD, respectively; (c) photographs of three kinds of R-CD dilute ethanol solution under daylight and 365 nm UV light. (d) Schematic representation, (e) UV–vis absorption spectrum and PL emission spectra of the preparation of R-CDs. Inset: photographs of solid state and liquid state R-CDs under daylight and UV light. (f) Preparation and working mechanism of NIR-emissive S, Se-co-doped CDs. (g) Schematic diagram of the preparation and growth mechanism of R-CDs. (g) Schematic illustration of highly efficient green- and red-emissive switching CDs doped into MTES and APTES to form CDs/gel glasses. Reprinted and adopted with permission from Ref. [25,78,81,85,87,89]. (Copyright 2017, 2018 and 2019 Wiley and Sons and Copyright 2018 and 2019 American Chemical Society and Copyright 2018 Springer.). (A colour version of this figure can be viewed online.)

and finally obtained highly water-dispersible CDs, which exhibited a broad absorption band from 400 to 700 nm and a strong deep-red emission centered at 680 nm. Encouraged by this finding, the same group used another conjugated polymer, polythiophene phenylpropionic acid (PPA), as the carbon source, and prepared novel CDs with a broad absorption band from visible to NIR regions and red emission centered at 640 nm [83]. In 2017, through hydrothermal treatment of polythiophene (PT2) and diphenyl diselenide in an alkaline solution at 180 °C for 24 h, Zhang's group synthesized S, Se-codoped CDs with excitation wavelength-independent NIR emissions peaking at 731 and 820 nm (Fig. 5f) [84]. In 2019, using polythiophene derivatives containing a number of benzene ring structure and alkyl chain as reactants, Zhou's group presented a doped crystalline CD with the maximum fluorescence emission at 700 nm via a hydrothermal method [85]. Based on detailed characterization and analysis, it is found that the length of alkyl chain regularly affects the emission wavelength of final products, which provides a new way to design CDs with specific light emission waveband at the molecular structural levels.

In addition to these simple aromatic compounds above, some other complex organic molecules containing two or more benzene rings are also proven to be ideal precursors for producing CDs with R/NIR or multicolor emissions. In 2017, by innovating a sequential dehydrating condensation and dehydrogenative planarization method (DCDP), Yang's group achieved the fabrication of 53% efficient R-CDs emitting at 628 nm from 1,3-dihydroxynaphthalene (Fig. 5g) [86]. Particularly, they deduced that one molecule of 1,3-dihydroxynaphthalene acting as the smallest sp^2 domain, could form uniformly large sized conjugated sp^2 cluster with pendent OH groups at the edge sites via controllable DCDP approach, consequently resulting in the strong red emission. Thereafter, with a solvent-engineered molecule fusion strategy, Wu and coworkers reported multi-color fluorescent CDs with high QYs of 28–72% and production yields of 50–92% using 1,3,6-trinitropyrene as the precursors [87]. The differences of these CDs in particle size, composition, and functional groups were believed to be responsible for their PL variations. In 2018, Zhou's group synthesized R-CDs with the absolute QY as high as 80% in NaOH solution (0.1 M) using 3,4,9,10-tetranitroperylene that was obtained by refluxing perylene with HNO_3 as carbon source [88]. Remarkably, those R-CDs could be developed into green emissive CDs by adjusting their surface electronic state without addition of an alkali. In addition, the highly efficient PL emissions of G-CDs and R-CDs could be demonstrated by respectively doping them into a highly transparent matrix of methyltriethoxysilane (MTES) and 3-triethoxysilylpropylamine (APTES) to form CDs/gel glasses, which exhibited high QYs of 80% for green emission and 78% for red emission, as shown in Fig. 5h.

Overall, laboratory-produced chemical reagents (summarized in Table 1), including ones with or without aromatic ring, are the dominating precursors for the preparation of highly luminescent CDs with R/NIR or multicolor emissions due to a wide range of alternatives and well-defined molecular structures. However, this kind of bottom-up synthetic strategy typically has several shortcomings. First, these as-prepared CDs are always a mixture with extremely complicated structures or compositions because of the high chemical reactivity and various reaction pathways [47]. Such a fact poses significant challenges to produce purified CD products on a large scale and to make clear the blurred PL mechanisms of CDs. Second, these adopted organic compounds, especially the ones containing big aromatic ring with well-known high toxicity, may have potentially hazardous influence on the environment and humans owning to their incomplete conversion into CD products during preparation [5]. Last but not least, phenylamine and phenol derivatives are easily oxidized in ambient environments, and as such, harsh air-free and low-temperature storage conditions are demanded, which may increase the synthesis or application cost to a certain extent [89]. As a result, it remains a challenge to massively synthesize long-wavelength or multicolor emission CDs with high emission efficiency from green and cheap precursors in an eco-friendly and cost-effective manner.

2.4. Biomass

Biomass, as a kind of eco-friendly and renewable natural products, contain abundant carbohydrates necessary for CD synthesis; therefore, they are also selected as a good carbon source for the preparation of CDs with R/NIR or multicolor emissions. In 2017, Li and coworkers reported a green and simple synthesis of bright self-passivated R-CDs by one step solvothermal treatment of spinach at 150 °C for 6 h [90], as shown in Fig. 6a–c. The R-CDs were 3–11 nm in size, and exhibited excitation-independent PL emission at 680 nm with a QY of 15.34%, which could be attributed to porphin structure attached onto the R-CD surfaces. In this regard, our group obtained excitation-independent luminescent CDs emitting at 631 nm through heating an ethanol solution of pulp-free lemon juice followed by purification with silica column chromatography (Fig. 6d–f) [91]. The resulting R-CDs are mono-dispersed with an average diameter of 4.6 nm, exhibiting a high QY of 28% in water, which were demonstrated to originate from their surface states and nitrogen-derived structures. In 2018, using a solvent-based extraction technique (Fig. 6g), Bhati et al. fabricated R-CDs from the leaves extract of a natural plant named Bougainvillea, which had excitation-independent emissions at about 678 nm with a QY of 40% [92]. Moreover, these R-CDs showed the ability to photodegrade the methylene blue within the ~120 min of sunlight irradiation, making them a potential nanomaterial for aqueous-phase photodegradation of pollutant dyes. In 2019, Hao's group developed second near-infrared emission CDs derived from watermelon juice via a hydrothermal route (Fig. 6h) [93]. The designed NIR-CDs possess emission located in 900–1200 nm, high QY (0.4%), high biocompatibility, and rapid renal clearance, making them desirable contrast agents for fluorescence bioimaging (FL imaging). These pioneering works have set a good example to prepare CDs with long-wavelength or multicolor emissions using biomass as carbon source. However, these biomass-derived CDs are subject to relatively low QYs and few available precursors in comparison with CDs derived from organic compounds.

3. Photoluminescence regulations over CDs with R/NIR or multicolor emissions

Understanding the PL mechanisms is key to design and synthesis of CDs with desired optical properties to meet the demands of a broad range of applications [73]. However, owning to the diversity and complexity of CDs in structure and composition, the origins of PL of CDs are not fully understood yet, which are highly dependent on particle size, surface functional group, graphitization degree, heteroatom doping, etc [21]. As such, this section will discuss the sound strategies for optimizing optical properties of CDs towards long-wavelength emission and decreased FWHM.

3.1. Regulations toward long wavelength emission

A large number of reports stated that PL emission intensity of CDs is primarily located in blue to yellow light regions, which is well outside of the zone that is desired for bioimaging applications. Enormous efforts have been devoted to extending the emission wavelength of CDs to R/NIR regions, through tailoring a bunch of attributes, such as particle size, surface state, and heteroatom doping [20].

Table 1
A summary of syntheses and FL properties of CDs with R/NIR or multicolored emissions.

Starting materials	Synthesis method	Ex/Em (nm)	QY(%)	Ref.
Graphite rods	Electrochemical etching	500/610	1.8 (water)	[43]
Carbon fibers	Acid oxidation	320-360/430-610	1.8–20.7 (water)	[44]
Graphene oxide	Chemical degradation	340-420/457-630	1-10 (water)	[45]
Coal pitch	Acid oxidation	366-495/400-630	5.4–10.1 (water)	[46]
CA, formamide	Microwave heating	540/640	22.9 (methanol)	[52]
CA, EDA, formamide	Solvothermal synthesis	560/627	53 (formamide)	[53]
CA, urea, DMF	Solvothermal synthesis	350-550/460-630	4.0–13.3 (water)	[94]
CA, urea, DMF	Solvothermal synthesis	400-575/430-630	12.9–52.6 (ethanol)	[54]
CA, urea, DMF, NH_4F	Solvothermal synthesis	710/772	9.8 (DMF)	[95]
CA, urea, DMF, DMSO	Solvothermal synthesis	732/760	10 (DMSO)	[96]
CA, urea, N,N-diethylformamide	Solvothermal synthesis	580/642	Null	[97]
CA, thiourea, acetone	Solvothermal synthesis	560/594	29 (ethanol)	[98]
CA, PEI, formamide	Solvothermal synthesis	550/640	Null	[55]
CA, neutral red	Hydrothermal synthesis	530/632	12 (water)	[57]
CA, DAN, H_2SO_4	Solvothermal synthesis	350-500/430-604	12-75 (ethanol)	[99]
CA, 5-amino-1,10-phenanthroline	Hydrothermal synthesis	560/630	67 (ethanol)	[58]
CA, 1-(2-pyridylazo)-2-naphthol	Solvothermal synthesis	320-470/375-585	31.6–46.5 (ethanol)	[59]
CA, 1,4,5,8-tetraminoanthraquinone	Hydrothermal synthesis	600/700	10.7 (DMF)	[100]
Glutathione, formamide	Microwave-assisted pyrolysis	420/683	16.8 (water)	[60]
p-PDA	Solvothermal synthesis	510/604	26.1 (ethanol)	[76]
p-PDA, H_3PO_4	Hydrothermal synthesis	530/622	11.2 (water)	[101]
p-PDA, urea	Hydrothermal synthesis	371-521/440-625	8.53–27.57 (water)	[33]
L-glutamic acid, o-PDA	Solvothermal synthesis	389-661/443-745	13-54 (ethanol)	[62]
L-cystine, o-PDA, ethanol	Solvothermal synthesis	540/595, 648	35.7 (ethanol)	[63]
Glycol, neutral red	Solvothermal synthesis	365/617	34 (ethanol)	[70]
Glucose, H_3PO_4	Heating reflux method	440/590	15% (dichloromethane)	[66]
o-PDA, HNO_3	Hydrothermal synthesis	540/630,677	31.54 (ethanol)	[77]
o-PDA, $AlCl_3$	Solvent-free carbonization	490/590, 640, 700	56.98 (ethanol)	[75]
o-PDA, Tris, H_2SO_4	Hydrothermal synthesis	420-600/445-611	21-64 (ethanol)	[69]
o-PDA, L-tartaric acid	Solvothermal synthesis	540/600	39.3 (ethanol)	[102]
o-PDA, dopamine, HCl	Hydrothermal synthesis	540/665, 710	26.28 (ethanol)	[74]
N,N-dipropyl-p-PDA, DMF	Solvothermal synthesis	560/645	86 (ethanol)	[25]
o-PDA, p-PDA, dopamine	Hydrothermal synthesis	573/640, 670	25 (ethanol)	[78]
Tris(4-aminophenyl)amine	Solvothermal synthesis	590/615	80.77 (ethanol)	[103]
Phloroglucinol, ethanol, H_2SO_4	Solvothermal synthesis	460-582/472-598	54-72 (ethanol)	[79]
Resorcinol, ethanol	Solvothermal synthesis	595/610	72 (ethanol)	[104]
Resorcinol, ethylene glycol, Na_3PO_4	Controlled carbonization	490/600	25 (water)	[80]
4-aminophenol, KIO_4, ethanol	Solvothermal synthesis	540/620	20.1 (water)	[81]
Polythiophene phenylpropionic acid	Hydrothermal synthesis	570/640	2.3 (water)	[83]
PT2, diphenyl diselenide, NaOH	Hydrothermal synthesis	460/731, 820	0.2 (water)	[84]
Polythiophene derivatives	Hydrothermal synthesis	530/700	3.92 (water)	[85]
1,3-dihydroxynaphthalene, KIO_4	Solvothermal synthesis	530/628	53 (ethanol)	[86]
1,3,6-trinitropyrene	Solvothermal synthesis	380-550/460-620	28-72 (toluene)	[87]
Perylene, HNO_3, NaOH	Solvothermal synthesis	560/610	80 (ethanol)	[88]
1,3,5-benzenetrithiol, H_2SO_4	Solvothermal synthesis	552/586	31.82 (ethanol)	[105]
1,4-phenylene diisocyanate, DMF	Solvothermal synthesis	495/604	33.7 (ethanol)	[106]
Spinach, ethanol	Solvothermal synthesis	420/680	15.34 (water)	[90]
Lemon juice, ethanol	Solvothermal synthesis	533/631	28 (water)	[91]
Bougainvillea leaves extract	Microwave charring	420/678	40 (water)	[92]
Watermelon juice	Hydrothermal synthesis	808/925	0.4 (water)	[93]
Taxus leaves, acetone	Solvothermal synthesis	413/673,722	59 (DMSO)	[107]
Manganese(II) phthalocyanine	Solvothermal synthesis	690/745	Null	[108]
cyanine dye, poly(ethylene glycol)	Solvothermal synthesis	720/820	5.2 (ethanol)	[109]

3.1.1. Particle size

Alike traditional QD semiconductors, CDs can exhibit a size-dependent quantum-confinement effect on their PL properties. Through increasing particle size, energy gaps of CDs can be reduced, thereby leading to a red shift in emission wavelength, which is essentially originated from the bandgap transition of conjugated π-domains in the sp^2-carbon-constructed core [99]. In 2017, Qu and coworkers prepared full-color emissive CDs with CA and urea by altering the reaction solvents in solvothermal conditions (Fig. 7a) [110]. Morphological and structural examinations reveal that the dehydration and carbonization reactions were gradually accelerated in water, glycerol, and DMF, resulting in the progressive growth of particle sizes from 1.7, 2.8–4.5 nm and red-shifted emission bands from 448, 550–638 nm. Such experimental findings led to the conclusions that the quantum confinement effect dominates the tunable bandgap emissions of CDs over surface/defect states, which is also proposed by Rogach's group in 2019 [111]. As shown in Fig. 7b, they produced a series of solid-state fluorescent CDs with blue, green, yellow, and orange colors through controlling the number density of seed CDs and reaction time. The distinct red shift of PL maxima is ascribed to the changes of the extent of the π-conjugated domains of increasingly larger particles, as well as increasing amount of graphitic nitrogen dopant in larger particles. In addition to experimental evidence, particle size-dependent emission was demonstrated by theoretical modelling. Chen's group used density-functional theory (DFT) and time-dependent DFT to calculate the emission wavelength of pristine zigzag-edged CDs with different diameters [112]. Results reveal that the CDs emitted tunable colors from blue to NIR linearly depending on size of CDs (0.46–2.31 nm), which is related to the

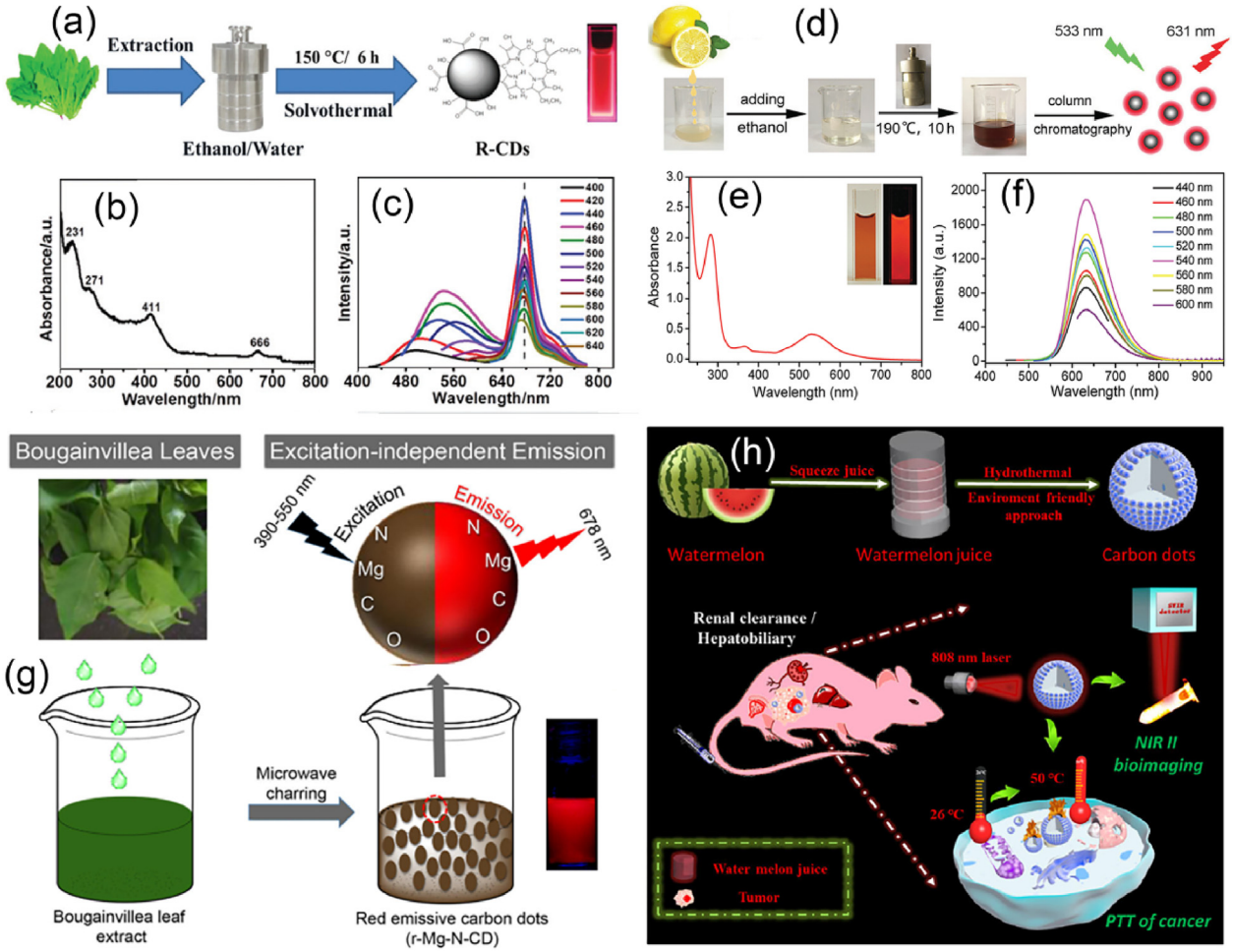

Fig. 6. (a) Synthesis diagram, (b) UV–visible absorption, and (c) PL emission spectra (III) of R-CDs. (d) Illustration of the preparation process, (e) UV–visible absorption, and (f) PL emission spectra of the R-CDs from lemon juice. (g) Schematic diagram showing the simple synthesis of red emissive Mg, N-co-doped CDs. Inset: photograph of R-CDs aqueous solution under UV light. (h) Schematic illustration of the synthesis of NIR-II emitting CDs for rapid renal clearance NIR-II bioimaging and photothermal therapy of cancer. Reprinted and adopted with permission from Refs. [91–94]. (Copyright 2017 and 2017 Royal Society of Chemistry and Copyright 2018 and 2019 American Chemical Society.). (A colour version of this figure can be viewed online.)

decrease in band gap resulting from π electron delocalization within the sp^2 domain. It should be noted that term "particle size" highlighted herein refers to inner effective conjugation length or sp^2 domain size in carbon cores, rather than physical dimensions of CDs that include a conjugated graphite core and an amorphous shell consisting of some functional groups as observed from TEM [113].

3.1.2. Surface states

Distinguishing from the quantum size effects, surface states are a complicated system which involves both carbon backbones and connected functional groups within a CD. Their energy gaps, where electrons and holes recombine to emit fluorescence, are highly associated with the extent of the π-electron system and surface chemistry [10]. Thus, through surface functionalization, post-oxidation, and extending size of the conjugated π-domain, new energy levels can be created between HOMO and LUMO, consequently allowing PL modulation of CDs toward R or NIR regions. In 2018, through modifying surface of orange emissive CDs with molecules or polymers rich in sulfoxide/carbonyl groups, Qu's group realized 10% efficient NIR emission at 760 nm under NIR excitation [96]. The attached S=O and C=O functional groups onto the basal planes of outer layers resulted in the occurrence of additional discrete energy levels due to increasing degree of surface oxidation, thereby contributing to the NIR absorption band and enhanced NIR fluorescence (Fig. 7c). Afterwards, Zhen et al. developed a simple approach to engineer the surface states of blue emissive CDs by conjugating them with vitamin C and acetaldehyde, and realized controllable red shifts of 175 nm and 285 nm in emissions [114]. Further experimental characterization results unveil that C=O and C=N related groups as sub-fluorophores are the origins of green and red emissions of CDs, respectively. Most recently, Wang's group prepared PL tunable CDs with blue, green, yellow, orange and red emissions based on thermal-driven Advanced Oxidation Process under facile green hydrothermal conditions [115]. In light of structure analysis and reported conclusions, they believed that these CDs are of surface-state emission, and that the red shift of PL emission is due to the bandgap narrowing which is indeed a result of the synergistic effect of larger π-electron system and higher content of graphite nitrogen (Fig. 7d). Though engineering surface state has been proven to be an efficient way to redshift PL emission of CDs, the knowledge of surface state remains inadequate, especially what the surface states of CDs are, and what the relationship is between surface states and their optical properties. Therefore, more attention should be cast upon those unknown facts, which are beneficial to the directional

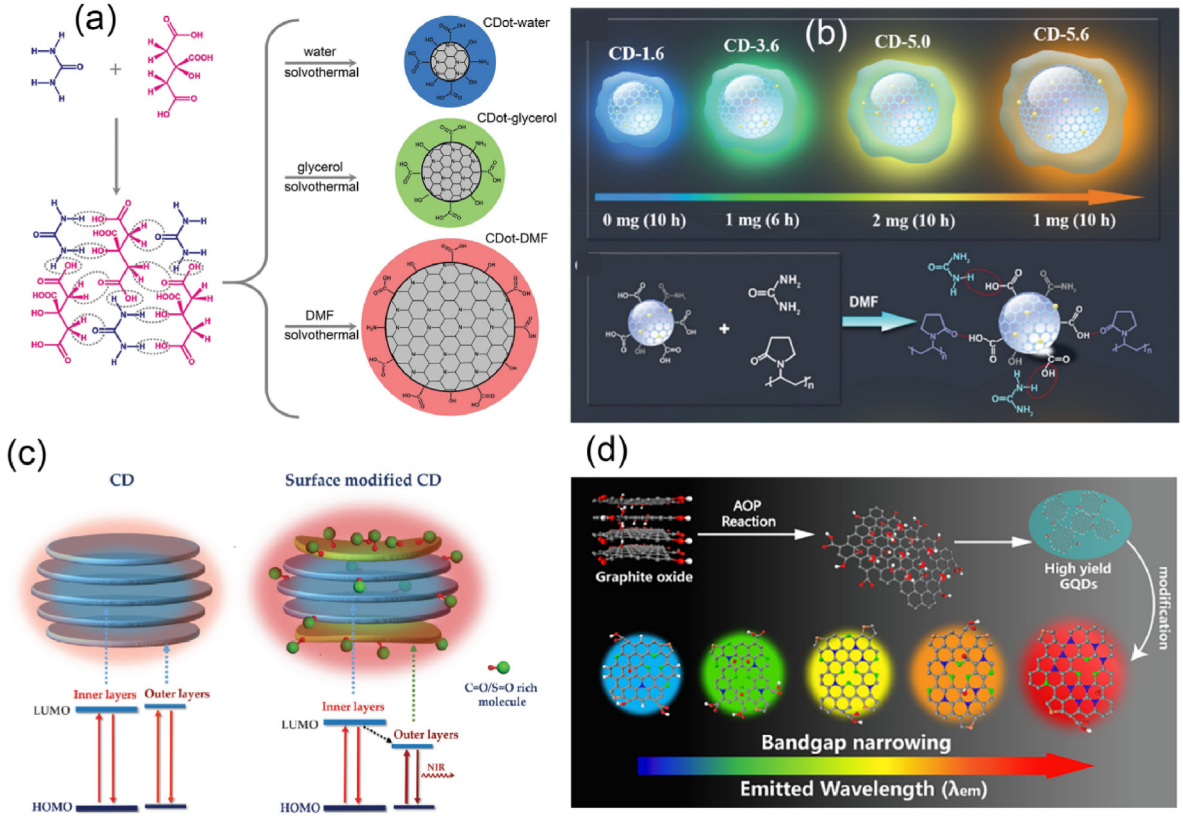

Fig. 7. (a) Schematic of a possible growth mechanism for full-color emissive CDs from CA and urea by using different reaction solvents in solvothermal conditions. (b) Schematic representation of four different selected sizes and the different extent of π-conjugated domains of the resulting CDs (upper); seeded growth reaction leading to the formation of CDs, and the possible interactions of their surface capping groups with precursor molecules in solution (bottom). (c) Schematic illustration of a possible mechanism for surface engineering to generate the NIR absorption band and enhanced NIR emissions from CDs. (d) Schematic illustration of stripping graphite oxide flakes into multicolored CDs with different particle size and content of graphite nitrogen. Reprinted and adopted with permission from Ref. [96,97,100,and102]]. (Copyright 2017 2018, and 2019 Wiley and Sons and Copyright 2020 Elsevier Ltd.). (A colour version of this figure can be viewed online.)

syntheses of CDs with desired optical properties.

3.1.3. Heteroatom doping

Apart from the three aforementioned mechanisms, heteroatom doping is an effective way to substantially tune the emission wavelength of CDs [40]. Up to now, many types of heteroatoms have been reported to induce remarkable PL redshifts of CDs by tailoring their structural and electronic properties. N doping, in forms of amino, pyridinic, hydrazine, and graphitic N, is the most common doping type that induces PL redshift of CDs. For instance, Otyepka and coworkers prepared full-color-emission CDs through heating a formamide solution of urea and CA, followed by column chromatography separation based on the surface charge discrepancy of CDs [94]. The largest amount of N exists in blue-emissive and green-emissive CDs in the form of amine/amides, whilst graphitic N dominats in yellow-emissive and red-emissive CDs. The increased amount of graphitic N in the CD structure, which is an electron-donating element, could generate midgap states between HOMO and LUMO, thus resulting in obviously redshifted absorption and emission (Fig. 8a). In 2018, through a one-step microwave-assisted hydrothermal treatment of same precursors, Ogi's group produced pyrrolic-N-rich CDs that shows strong NIR absorption centered at 650 nm [116]. The increased amount of pyrrolic N functional groups in as-prepared CDs leads to a high electron density and delocalized electron waves spreading through CD surface, thus enabling the redshift of absorption wavelength to the first NIR window region. Moreover, heteroatom co-doping was also developed to regulate optical behavior of CDs. Using o-PDA and DMF as raw materials, Gao et al. synthesized multicolor emissive N,S-codoped CDs from green to red via a simple solvothermal route [117]. Results reveal that S doping significantly increases the content of graphitic N, facilitating PL shifting from green to yellow. Subsequently, water engineering is able to enhance surface oxidation degree and generate carboxyl group, which further narrows the band gap, resulting in PL shifting from yellow to red. Therefore, N and S doping as well as carboxyl group synergistically reduce the energy gaps of prepared CDs, thus contributing to the red-shift of fluorescence, as shown in Fig. 8b. Similarly, Ren's group synthesized B-, N- and S-co-doped R-CDs by one-step hydrothermal treatment of 2,5-diaminobenzenesulfonic acid and 4-aminophenylboronic acid (Fig. 8c) [118]. In that study, doped B and S demonstrate reduced nonradiative recombination, and N doping reduces bandgap and ensure bandgap uniformity, synergistically leading to the intensive red PL emission with a narrowed FWHM.

In addition to nonmetallic atoms, metallic ions, such as Cu^{+}, Zn^{2+}, Mn^{2+}, Hg^{2+}, and Fe^{3+}, are also used as dopant to tune PL behavior of CDs. The introduced metallic ions could contribute electrons to CDs through forming chelate with electrophilic groups of CDs, which changes their internal electronic environments, thereby resulting in improved charge density and tunable electron energy levels. In 2016, Liu's group designed solid-state Cu-doped CDs with an excitation-independent red emission at 620 nm through microwave-assisted thermal treatment of an aqueous solution of N-(2-Hydroxyethyl) ethylenediamine-N, N, N-triacetic acid, tartaric acid, and L-cysteine [119]. By investigating emission mechanism with steady-state and time-resolved PL spectroscopy, it

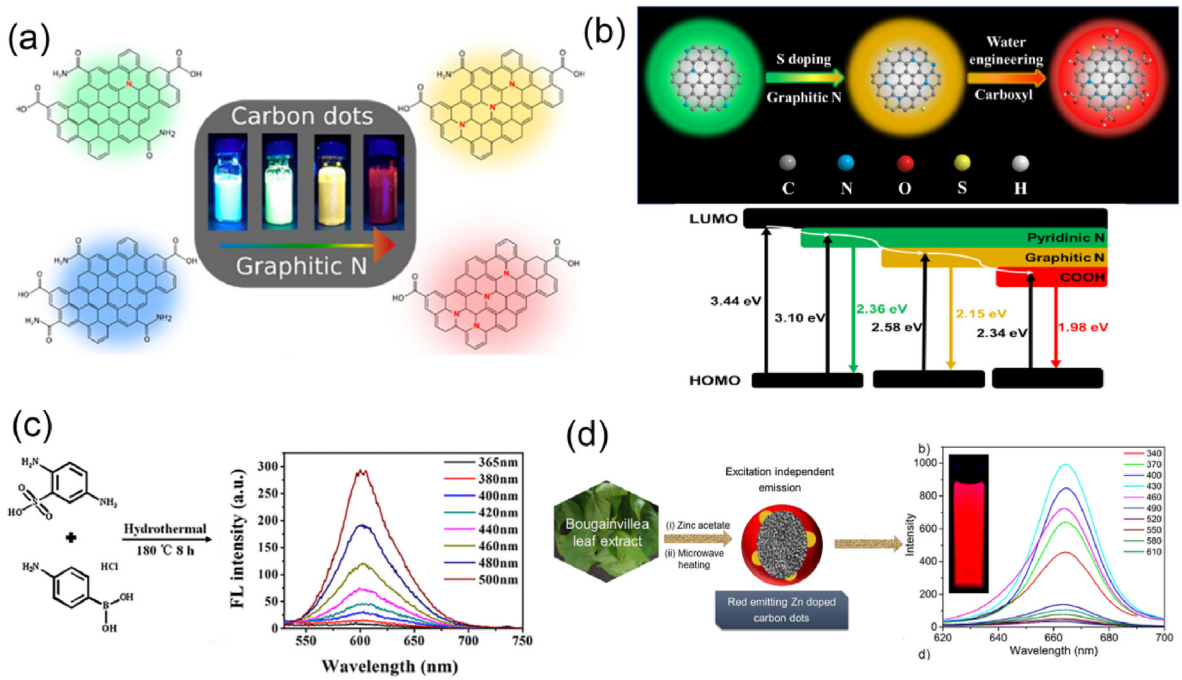

Fig. 8. (a) Schematic alignments of red fluorescence in CDs trigged by graphitic nitrogen. (b) Schematic diagram of the possible (upper) structure models and (bottom) energy level of the PL-tunable CDs. (c) Synthesis rout of B,N,S, co-poped-R-CDs and their PL emission spectra. (d) Schematic illustration showing the simple synthesis of red-emitting Zn-doped CDs and their PL emission spectra excited by different wavelengths of light. Reprinted and adopted with permission from Refs. [103,105,106,and108]]. (Copyright 2017, 2017, and 2018 American Chemical Society and Copyright 2020 Elsevier Ltd.). (A colour version of this figure can be viewed online.)

was observed that R-CDs had an excited-state lifetime in the range of microseconds, indicating that the red emission may be from the spin-forbidden transition of the triplet parentage of Cu(I)-thiolate complexes. In 2018, using Bougainvillea as carbon source and zinc acetate as passivation agent, Khare et al. obtained highly efficient Zn-doped R-CDs with a QY of up to 72% via a simple and green synthesis process (Fig. 8d) [120]. In comparison with the control sample without Zn doping, it was confirmed that the introduced zinc oxide could passivate surface of CDs, which not only redshifts the emission peak toward long-wavelength region but also improves radiation recombination probability. As a consequence, the as-obtained Zn-doped CDs show ultra-bright excitation-independent red emissions along with excellent solubility and stability in aqueous media as well as excellent photostability. Meanwhile, rare earth ions, such as La^{3+}, have also been incorporated into internal structure of CDs to tune their fluorescence properties [121]. The introduced La^{3+} existed in carbon core in the bond of La-O, and could cause local structure change, narrowed energy gap and increased charge transfer, thereby exhibiting a remarkable PL redshift and a significant emission intensity enhancement. Though metallic ion doping greatly enhances the optical performance of CDs, it also brings about some serious problems, especially the increased preparation cost and toxicity, which would hinder their further application in biotechnology.

3.1.4. Other factors

In addition, other factors such as pH, concentration, solvent, and even aggregation can also show important effects on PL regulations of CDs [21]. As previously noted, Yuan et al. prepared pH-responsible CDs from electrolysis of graphite rods [122], and found that upon varying pH value from 1 to 14, the CD solution displays a distinct red shift both in absorption and PL emission spectra (Fig. 9b and c), which is confirmed by the clear PL color change from light yellow to brown and to red under an UV lamp (Fig. 9a). The red emission was attributed to the structural changes from lactone to quinone at high pH values (above 12). The unique optical properties made them an ideal candidate as a dual sensing probe for intracellular pH value and temperature. Similarly, through simply changing solvents, Xie's group reported single-type CDs with continuously tunable multicolor emission from green to red (Fig. 9d), which allows them to be applied in fabricating trichromatic red LED and white LED [123]. The increase in solvent polarity causes a decrease in energy levels between HOMO and LUMO, and therefore resulted in the bathochromic shift of fluorescent emission. In the study of aggregation-dependent emission of CDs, Liu's group obtained self-quenching-resistant dual-color CD composites with the characteristic peaks located at nearly 440 and 600 nm [124]. Meanwhile, they supposed the decreased interparticle distance in aggregation state could effectively facilitate the process of resonance energy transfer and reabsorption, resulting in the redshifted PL emission, as shown in Fig. 9e. Most recently, Chen's group found that the PL color of CDs solution changed from blue to red over the whole visible spectrum as CDs concentration increased from 0.1 to 100 mg/mL (Fig. 9f and g) [125]. This concentration-dependent emission was mainly caused by the synergistic effect of the band gap narrowing induced by increasing CD concentration and content of C–O–C/C–O–H groups.

Overall, the quantum size effects, surface states and atom doping all account for the overwhelming majority of PL redshift in CDs. However, it should be noted that those factors generally show synergistic contributions to the optical properties of CDs due to their overlapping relationships with structure and composition of CDs. Furthermore, it is a challenge to decouple the influence of any individual factor from the others. Thus, fully understanding PL mechanisms and desirably engineering PL properties of CDs remain a great technical challenge.

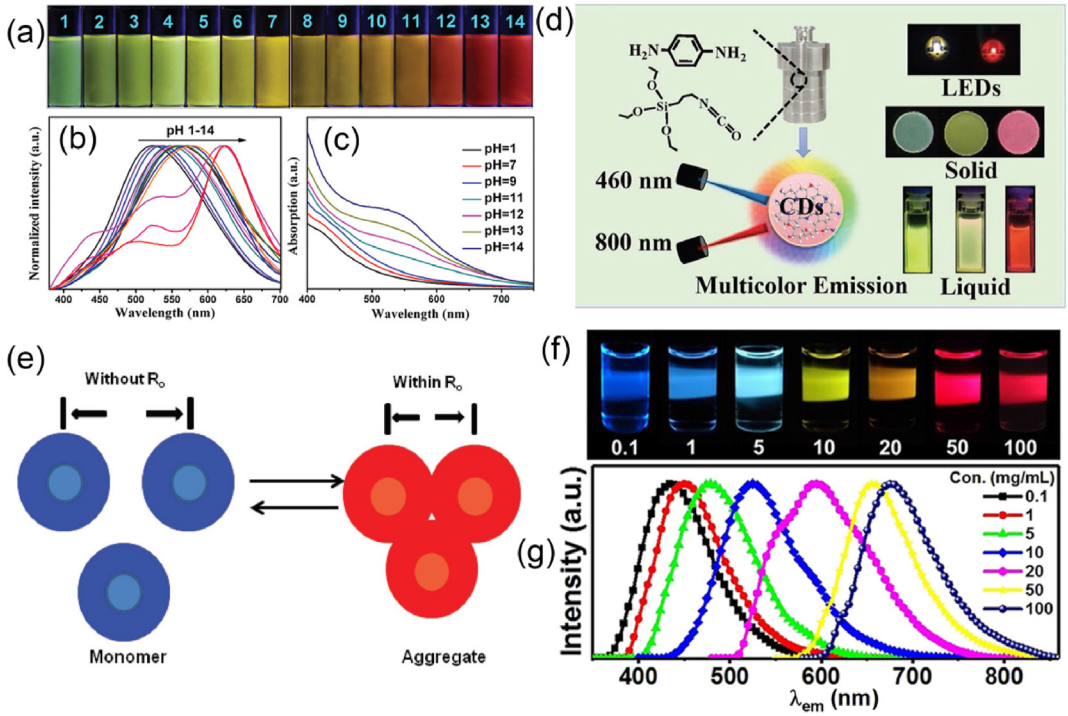

Fig. 9. (a) Fluorescence images under UV light, (b) normalized PL spectra and (c) UV–visible absorption spectra of the CDs in universal buffer solution at different pH values. (d) Schematic illustration of the preparation of multicolored CDs and their applications in fabricating trichromatic WLED and red LED. Inset: photographs of liquid-state and solid-state multicolored CDs under UV light. (e) Schematic illustration of aggregation-induced PL redshift of CDs. (f) Fluorescence images of multicolored CD solutions with indicated concentrations excited at their optimal excitation wavelengths, and corresponding (g) normalized PL spectra. Reprinted and adopted with permission from Ref. [110–113]. (Copyright 2018 Royal Society of Chemistry and Copyright 2017 and 2018 Wiley and Sons and Copyright 2019 American Chemical Society.). (A colour version of this figure can be viewed online.)

3.2. Regulation toward decreased emission bandwidth

Typically, the PL spectra of CDs are usually broad with a FWHM exceeding 80 nm because of their multiple emission centers that may stem from a broad size distribution, abundant structural defects, and various heteroatom doping [126]. Such a broad bandwidth emission is far inferior to that of Cd^{2+}/Pb^{2+}-based QDs, and has severely hindered the application of CDs in higher-contrast bioimaging. To solve this problem, scientists have put painstaking effort into initiating extensive investigations on the topic and successfully achieving a few CDs with FWHM values of 20–40 nm, which involves weakening the electron-phonon coupling, reducing the surface defects, or narrowing size distribution. In 2018, Yuan et al. synthesized highly efficient multicolored CDs with an unprecedented narrow bandwidth of 29 nm by thermal treatment or refluxing of phloroglucinol in ethanol or H_2SO_4 (Fig. 10a–d) [79]. The as-prepared CDs exhibit a triangular shape, a highly crystalline graphene structure, and a temperature-dependent emission narrowing phenomenon. Accordingly, they concluded that the unique triangular structural rigidity and highly delocalized charges could dramatically reduce electron-phonon coupling interactions of the CDs surrounded by hydroxy groups, thus leading to a high color-purity bandgap emission, which aligns well with the follow-up DFT calculations. Inspired by this finding, the same group then achieved another kind of pure red emission CDs showing a FWHM of 33 nm with a QY of 75% by simply repacling precursor phloroglucinol with resorcinol (Fig. 10e and f) [104]. In 2019, Han and coworkers prepared highly efficient orange emission CDs exhibiting a high QY of 82% and a narrow FWHM of 30 nm via a one-step ethanol solvothermal treatment of 1,4-diaminonaphthalene followed by silica column chromatography separation (Fig. 10g and h) [127]. By comparing those CDs with other three collected CDs with broad emission bandwidths, it was found the uniform size distribution results in a narrow bandwidth. Thereafter, Jia's group synthesized efficient R-CDs emitting at 612 nm with a QY of 84% and a narrow emission linewidth of 27 nm by adopting a conjugated aromatic amine precursor (tris(4-aminophenyl)amine, TAPA) and introducing oxidative radical reagents (Fig. 10i and j) [103]. Judging from control experiments and structural studies, it was demonstrated that the use of highly conjugated precursors endowed the resultant CDs with fewer structural defects and a more homogeneous structure, thus resulting in better PL performance in terms of a high PLQY and narrow FWHM. Very recently, Yang's group synthesized highly efficient deep red emissive CDs with unprecedented FWHM of 20 nm (Fig. 10k–n) [107]. Detailed characterizations identified that CDs have unique polymer characteristics, consisting of carbon cores and the shells of polymer chains, and π conjugated system formed with N heterocycles and aromatic rings govern the single photoluminescence (PL) center, which is responsible for high QY in deep red emissive CDs with narrow FWHM. These few examples revealed that the synthesis of CDs with narrow FWHM highly depends on the clever choice of molecular precursors. And it remains a great challenge to regulate FWHM due to lack of sufficient knowledge on the mechanisms underlying the broad fluorescence spectra of CDs. Remarkably, in the most recent work, Lu's group provided a surface-engineered route to reduce FWHM of CDs [128]. In that study, they first explored the effect of oxygen-containing functional groups on spectral linewidth using DFT calculations and found that wavefunction polarization arising from the thermal vibrations of oxygen-containing functional groups contributes to spectral broadening. Following this, they designed an additional surface

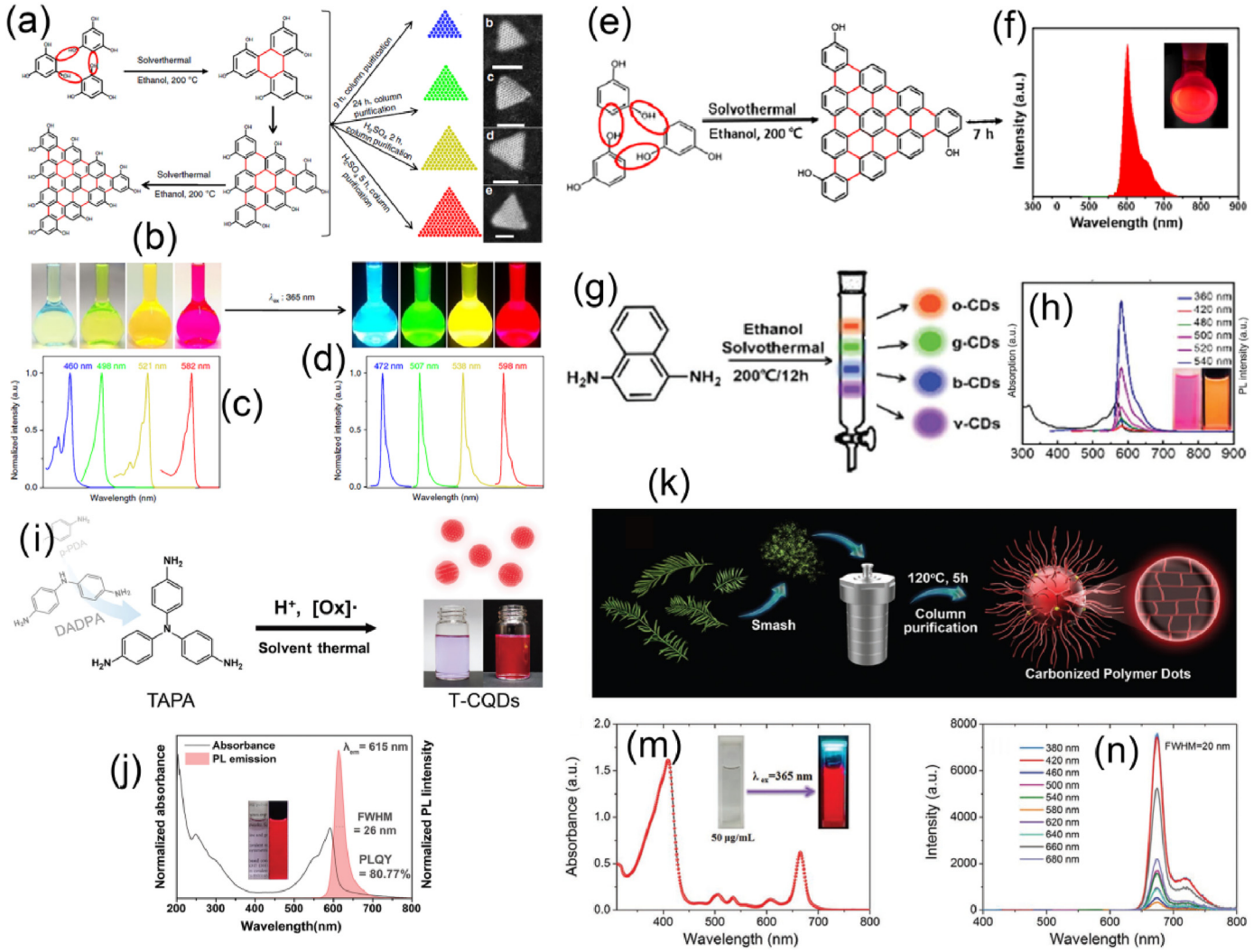

Fig. 10. (a) Synthesis route, TEM images, (b) UV OFF and UV ON optical images, (c) normalized Uv–vis absorption and (d) PL spectra of the multicolor narrow bandwidth emission triangular CDs, respectively. (e) The synthesis of R-CDs by solvothermal treatment of resorcinol and (f) corresponding PL spectra. (g) The synthesis of orange emitting CDs by solvothermal treatment of 1,4-diaminonaphthalene followed by silica column chromatography separation, and their (h) corresponding PL spectra. (i) Schematic illustration of the synthesis, (j) UV–vis absorbance and PL emission spectra of R-CDs. Inset: photographs of R-CD aqueous solution under daylight and UV light. (k) Schematic illustration of the preparation, (m) absorption spectra, and (n) PL emission spectra of NIR-CDs; inset: the photograph of NIR-CDs in acetone solution under daylight and UV light. Reprinted and adopted with permission from Ref. [80,115–118]. (Copyright 2018 Nature Publishing Group and Copyright 2019 Springer and Copyright 2019 and 2020 Royal Society of Chemistry and Copyright 2020 Wiley and Sons.). (A colour version of this figure can be viewed online.)

amination step using ammonia liquor and hydrazine hydrate under high temperature to further eliminate the oxygen-containing functional groups. As a result, they achieved high luminescent, deep-blue narrow-bandwidth emissive CDs with a FWHM of 35 nm, which were used to fabricate high-performance deep-blue LEDs with a maximum luminance of 5,240 cd m^{-2} and an external quantum efficiency of 4%.

4. Biomedical applications of R/NIR-CDs

Apart from general properties of CDs, R/NIR-CDs also show some unique advantages, such as long-wavelength excitation and emission which could be able to penetrate animal bodies deeply without disturbance of strong tissue autofluorescence [129]. As a consequence, the applications of R/NIR-CDs in biomedical fields, such as bioimaging, sensing, drug delivery/release, and photothermal/photodynamic therapy, have been a hot area of research in recent years.

4.1. Bioimaging

4.1.1. Down-conversion FL imaging

Compared to short wavelength emissive CDs, R/NIR-CDs have more advantages in optical imaging, such as deep tissue-penetrating depth, minimal photodamage to biological samples, minimum autofluorescence and light scattering by tissues, as well as great imaging contrast and spatial resolution [29]. At present, reports on deep R/NIR emissive CDs are continuously increasing, and their applications in visualizing biological systems both *in vitro* and *in vivo* have been explored. Regarding *in vitro* cell imaging, a large number of R/NIR-CDs were incubated with various cancer cells to test their labeling application potential. Results demonstrate that most R/NIR-CDs could accumulate in cell membrane and cytoplasm [95,130,131]. For instance, our group employed highly efficient R-CDs as a luminescent probe to elucidate the mechanism behind the transport of CDs [53]. The results in Fig. 11a show that, as incubation time and temperature increase, R-CDs could pass

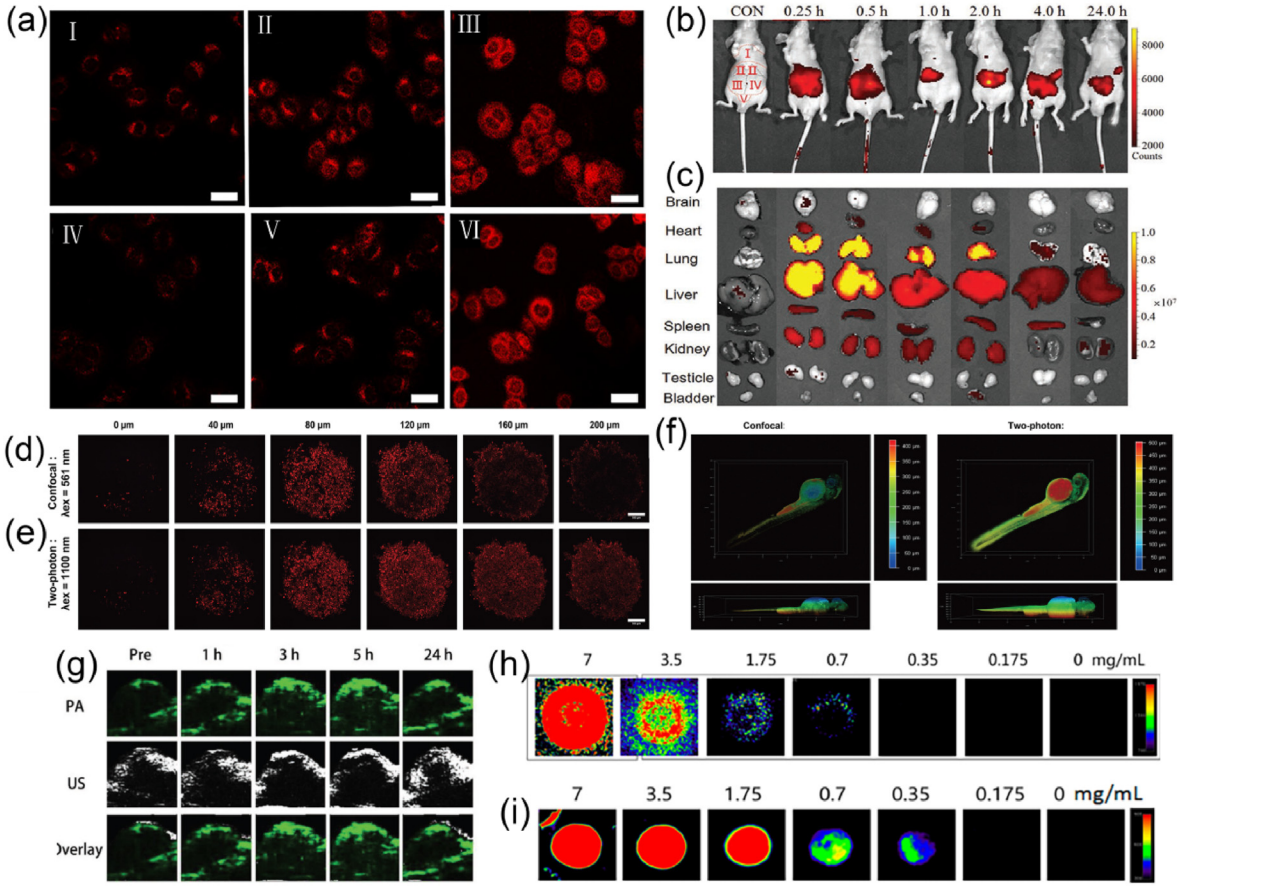

Fig. 11. (a) CLSM images of HeLa cells incubated with 50 mg/mL of the R-CDs for 0.5 (I), 1 (II), and 2 h (III), respectively; CLSM images of HeLa cells incubated for 2 h at 4 (IV), 25 (V), and 37 °C (VI), respectively. Excitation wavelength is 514 nm and scale bar represents 50 μm. (b) *In vivo* imaging and (c) real-time ex vivo imaging of supine nude mice with intravenous injection of NIR-CDs at different time points. (d) Confocal and (e) TP imaging results of a Hela cell tumor spheroid stained with R-CDs. (f) Confocal (left) and TP imaging (right) results of zebrafish larvae stained with R-CDs. (g) PA B-scan images of 4T1 tumors in mice after intravenous injection of NIR-CDs at different time points. PA imaging of the aqueous solution of (h) NIR-CDs and (i) cetuximab-modified NIR-CDs with indicated concentrations under 686 nm. Reprinted and adopted with permission from Refs. [53,112,113,128and129]. (Copyright 2017 and 2018 American Chemical Society and Copyright 2019 and 2020 Wiley and Sons and Copyright 2020 Royal Society of Chemistry.). (A colour version of this figure can be viewed online.)

through cell membrane and gradually accumulate in cytoplasm, thereby emitting strong red luminescence. Such a result indicates that both energy-dependent endocytosis and passive diffusion involved in cellular uptake of R-CDs, just like many other nanoparticles [132]. Furthermore, there are few R/NIR-CDs that were reported to reside in particular sites of cells, such as lysosome [133], and nucleolus [134]. Wu's group explored intracellular localization of R-CDs in A549 cells through observing the fluorescence signal of R-CDs under a confocal laser scanning microscope (CLSM) [134]. It is evident that nuclei were illuminated with bright red fluorescence at each time point, indicating selective accumulation of R-CDs in nucleoli, which is due to their selective binding to ribonucleic acid. At the same time, the applications of R/NIR-CDs in *vivo* imaging was also verified. By using a poly(vinylpyrrolidone) (PVP)-functionalized CDs with both excitation and emission in the NIR regions (λ_{ex} = 715 nm, λ_{em} = 760 nm), Rogach's group performed NIR fluorescence imaging in live mice [96]. After a gavage injection of NIR-CDs/PVP aqueous solution, a bright NIR fluorescence signal occurred in stomach of the mouse under 671 nm laser excitation, which could be easily distinguished from the background through a 800 nm longpass optical filter, indicating the fluorescence of NIR-CDs could efficiently penetrate mice skin and tissues. Very recently, by tail vein injection (dose: 20 mg kg^{-1}), Yang's group evaluated the *in vivo* biodistribution imaging of deep red emissive CDs in nude mice [107]. As shown in Fig. 11b, *in vivo* fluorescence images were collected at 0.25, 0.5, 1.0, 2.0, 4.0, and 24 h, respectively, under excitation of 640 nm laser light. At 0.25 and 0.5 h postinjection time points, clear and strong fluorescence emitting at 705 nm with excellent signal-to-noise ratio was clearly observed in the whole body of the mice. After 24 h of circulation, the fluorescence signal intensity became dramatically weak. Futhermore, organs fluorescence imaging collected at different time points postinjection was obtained to explore the biodistribution and excretion pathway of deep red emissive CDs. The results in Fig. 11c showed that the fluorescence intensity of the same dissected organ was gradually reduced as the extension of time, which was consistent with *in vivo* imaging. Besides, fluorescence signals of liver, lung, and kidney were much stronger than these of brain, heart, and testicle, and only few deep red emissive CDs were found in liver after 24 h circulation. Therefore, these results validated that the intravenously injected deep red emission CDs rapidly enter the whole body of mice by blood circulation and can be rapidly excreted from the body of post-imaged mice rather than accumulate at the injection sites.

4.1.2. Up-conversion FL imaging

Although down-conversion FL bioimaging exhibit unique advantages, it also suffers shallow tissue penetration and severe light

scatter, especially when compared with up-conversion FL bioimaging [29]. Some R/NIR-CDs exhibit multiphoton excited upconversion fluorescence under excitation of 800–2000 nm, which implies great application potential of NIR excitation in terms of deepened penetration, minimal photodamage, low autofluorescence and long observation time [15]. To date, a few reports were published regarding NIR light excited multi-photon imaging with CDs. For *in vitro* cell imaging, Liu and coworkers used R-CDs as imaging agents, and achieved two-photo (TP) FL imaging toward B16-F10 cells under 800 nm excitation [75]. Bright deep-red emission could be observed under confocal microscopy, indicating R-CDs were uniformly distributed into cytoplasm of B16-F10 cells. For *in vivo* fluorescence imaging, inspired by thermally activated upconversion NIR luminescence from CDs [135], Qu's group explored NIR upconversion luminescence imaging on a mouse model. After subcutaneous injection of NIR-CDs in DMF (40 μL, 40 ppm) at room temperature, bright up-conversion PL signal of NIR-CDs was captured on the back of the mouse under the excitation of 808 nm continuous laser light. It is noted that the above TP fluorescence imaging is achieved with NIR-I as excitation source, especially 800 nm. However, compared to NIR-II (>1000 nm) excitation, the penetration ability of 800 nm light is limited [24]. Consequently, R/NIR-CDs with excitation in NIR-II region are highly demanded for bioimaging. In this regard, Jia's group performed NIR-II light driven TP imaging both *in vitro* and *in vivo* [103]. As seen in Fig. 11d and e, after staining a HeLa cell tumor spheroid with R-CDs, a strong luminescence intensity remains at a penetration depth over 200 μm under excitation of 1100 nm, which is two times deeper than that of tumor spheroids under excitation of 561 nm. Meanwhile, use of R-CDs as contrast agent was examined for *in vivo* imaging in a TP model. With NIR-II excitation applied, the whole outline of a 96 hpf zebrafish larva was observed in a 3D reconstruction file with the maximum penetration depth of 500 μm (Fig. 11f). In contrast, only the near side of the larvae was imaged under a one-photo mode control when excited with visible light.

4.1.3. Photoacoustic imaging

In addition to fluorescence imaging, R/NIR-CDs show unrivalled application prospects in PA imaging based on NIR absorption [83]. Photoacoustic (PA) imaging relies on the phtotacoustic effect and combines deep tissue penetration of ultrasound imaging and high contrast of optical imaging. For example, Qu's group prepared NIR-CDs from CA and urea as carbon sources with dimethylsulfoxide as reaction solvent [136]. The as-prepared NIR-CDs exhibit a broad and strong absorption band from red to NIR region with a maximum absorption coefficient at 600 nm and a NIR mission peak at 720 nm. The feasibility of using NIR-CDs as an efficient NIR light-triggered contrast agent was examined for *in vivo* PA imaging. After intravenous injection into mice with 4T1 tumors (Fig. 11g), NIR-CDs were uniformly accumulated in tumor area through the enhanced permeability and retention (EPR) effect, exhibiting peak PA signals at 3 h post-injection in comparison with other tissues, which aligns well with the NIR FL imaging observations, demonstrating that the NIR-CDs can simultaneously act as FL and PA image agent for *in vivo* imaging. To enhance the PA signals of CDs in tumor, Zhu's group modified the surface of porphyrin-based N-CDs with cetuximab for precisely targeting cancer cells with overexpression of epidermal growth factor receptor (Fig. 11h and i) [137]. As expected, under NIR laser irradiation, the resulting NIR-CDs could significantly enhance PA amplitude signals and maintain a strong signal for 12 h in the mice bearing MDA-MB-231 breast cancer, which provides a long-term and accurate guidance for efficient photodynamic therapy for breast cancer. Overall, NIR absorbing/emission CDs display impressive potential in FL, TP, PA, and multimodel bioimaging. However, it remains a great challenge to regulate the absorption and emission wavelengths of CDs, especially in R to NIR regions, but enormous experimental results demonstrate that proper precursors, reaction solvents and separation techniques are the decisive factors.

4.2. Biosensing

As a versatile category of fluorescent nanomaterials, R/NIR-CDs have outstanding properties for both *in vitro* and *in vivo* biosensing applications owing to their significant advantages, such as flexible surface modification, superior photostability, excellent chemical stability, and excellent biocompatibility [18]. Recently, a large number of R/NIR-CDs-based sensing systems have been constructed based on analyte-induced fluorescence quenching or enhancement, which elicits high selectivity regarding metal ions, intracellular pH, small organic molecules, and organophosphorus pesticides.

4.2.1. Detection of metal ions

Metallic ions play important roles in various chemical and biological activities, yet the massive usage of metallic ions is harmful to the environment and public health [138]. Therefore, using R/NIR-CDs as a fluorescent nanosensor to detect metal ion pollutants in aqueous solution is meaningful [139]. Liu and coworkers developed a new colorimetric and fluorescent dual mode nanosensor based on R-CDs for the effective and fast detection of Fe^{3+} ions [118]. In their study, R-CDs show a high sensitivity towards Fe^{3+} in aqueous solution in a range of 0.3–546 μM with a detection limit of 90 nM (Fig. 12b and c), which is provided by quenching the red emission fluorescence via the formation of a stable nonfluorescence complex between surface functional groups of R-CDs and Fe^{3+}. Color of the R-CD solutions varied from red to blue with the increasing Fe^{3+} ion concentration, which is visible to the naked eye (Fig. 12a). Moreover, the designed nanosensor could be applied for efficient detection of Fe^{3+} in complex biological fluids and living cells within 1 min, implying a feasibility for real time detection of Fe^{3+}. Then, through employing a mixture of R-CDs and blue CDs (B-CDs) as ink by jet-printing on paper [140], Zhao's group constructed ratiometric fluorescent test papers for semiquantitive assay of Cu^{2+}, which exhibited a dose-sensitive color change from blue to red with a discernible scale as low as 25 nM Cu^{2+} ions. In that system, red fluorescence of R-CDs was maintained as a stable internal standard, whereas blue fluorescence of B-CDs was gradually quenched with addition of Cu^{2+} ions, which is ascribed to a specific spectral energy transfer between B-CDs to the Cu^{2+}–p-phenylenediamine complex at the surface of R-CDs. Importantly, the fluorescent test papers could meet the requirements of visual detection of Cu^{2+} ions in tap water and lake water samples with high accuracy and visual effect. Recently, Zhou's group reported a novel R-CDs-based fluorescent probe toward Pt^{2+}, Au^{3+}, and Pd^{2+} with corresponding detection of limits of 0.886 mM, 3.03 mM and 3.29 mM, respectively [57]. In the stduy of fluorescence quenching process, average FL lifetime of R-CDs was decreased from 1.41 to 0.41 ns after addition of Pt^{2+}, suggesting a fast electron transfer process between R-CDs and Pt^{2+} that caused dynamic quenching. However, no significant changes were evident in the fluorescent lifetime before and after adding Au^{3+} or Pd^{2+}, which indicates that the strong inner filter effect occurred between R-CDs and Au^{3+} or Pd^{2+}.

4.2.2. Detection of intracellular pH

Using R/NIR-CDs as a fluorescent probe, intracellular pH could be detected through monitoring the changes of fluorescence intensity, which is crucial for the understanding of physiological and

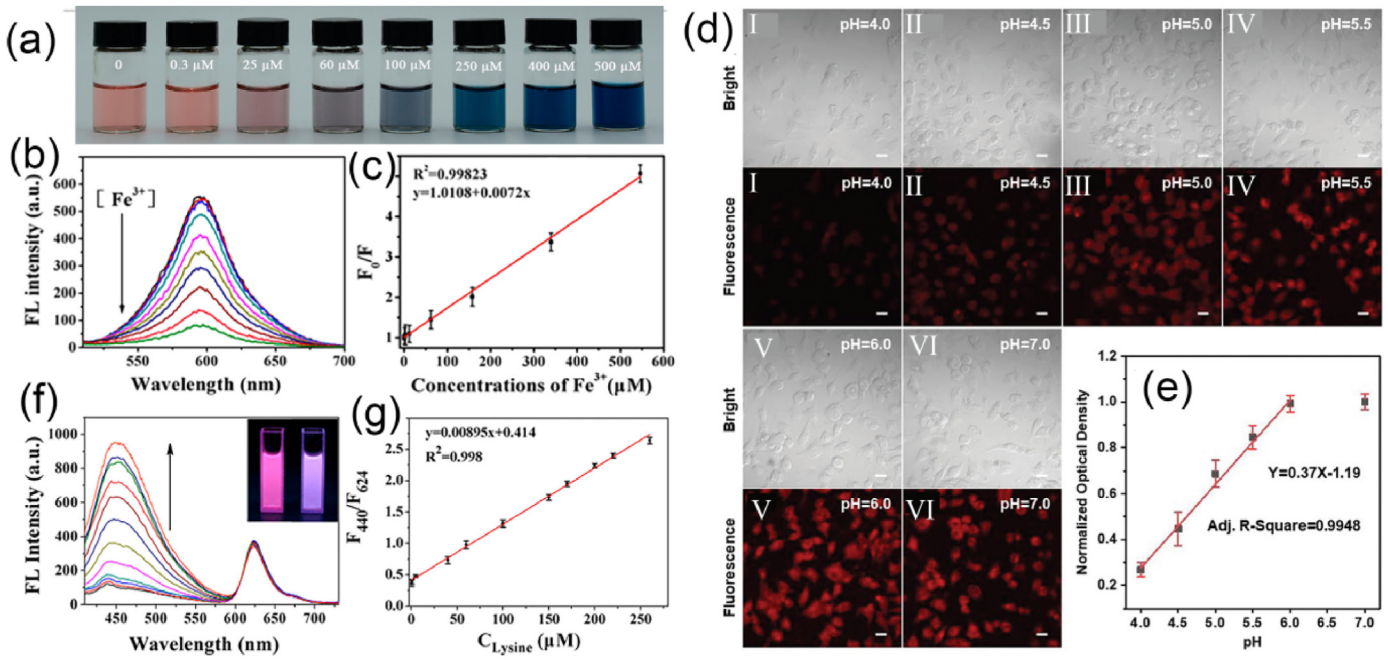

Fig. 12. (a) Photographs of R-CD aqueous solutions after adding various concentrations of Fe^{3+} under sunlight. (b) FL emission spectra of the R-CDs upon the addition of various concentrations of Fe^{3+} from 0 to 642 μM (I); (c) relationship between F_0/F and the concentration of Fe^{3+}, where F_0 and F are FL intensities of the R-CDs at 595 nm in the absence and presence of Fe^{3+}, respectively. (d) CLSM images of HeLa cells incubated with 100 μg mL−1 R-CDs in high-K^+ HEPES buffered solutions at different pH values (scale bar: 20 μm) (I-VI); (e) intracellular pH calibration curve of the R-CDs. (f) FL spectra of dual emission CDs after adding different concentrations of lysine (0.5–260 μM) in 100 mM buffer solution at pH 2.0; (g) linear relationship between F_{440}/F_{624} and the concentration of lysine, where F_{440} and F_{624} are FL intensities of the R-CDs at 440 and 624 nm in the presence of lysine, respectively. Reprinted and adopted with permission from Ref. [106,134and135]; (Copyright 2017 American Chemical Society and Copyright 2018 Royal Society of Chemistry.).

pathological processes [68]. In 2018, Xia and coworkers developed a modulated-polymerization method to produce pH-sensitive CDs with an excitation-independent red emission [141]. As pH value increased from 2 to 6, the PL intensity of R-CDs at 600 nm increased first and then reached a maximum value under excitation of 480 nm, giving a linear relationship between the PL intensity and the pH value, which was associated with the changes in the surface energy levels of the R-CDs. Such a pH-sensitive phenomenon made them an outstanding candidate for intracellular pH sensing (Fig. 12d and e). Later, using o-PDA, L-cystine and ethanol as raw ingredients, Xu's group prepared highly efficient N,S-co-doped R-CDs with an excitation-independent dual-emission at 595 and 648 nm [63]. Remarkably, the R-CDs exhibited excellent pH-responsive and reversible fluorescence in a wide PH value window of 1.0–13.0, enabling the application of R-CDs as a potential fluorescent pH sensing probe for environmental samples and living cells. Liu's group fabricated a R-CDs-based fluorescence probe for monitoring intracellular pH using a simple one-pot hydrothermal method [78]. The probe exhibits a pH-sensitive response in a linear range of 3.5–6.5, which is regulated via switching between aggregation and disaggregation of R-CDs. More importantly, by virtue of their high selectivity, excellent photostability, and low cytotoxicity, the R-CD probe could be successfully applied to sense and visualize pH fluctuations in cell, tissue, and zebrafish.

4.2.3. Detection of organic molecules

During the development of sensing by R/NIR-CDs, much progress has also been made in the detection of small molecules, which varies from amino acids to pesticides to organic dyes [21]. For instance, based on blue/red dual emissive CDs, Song et al. prepared a fluorescent probe toward Lysine in a "turn-on" mode [142]. As shown in Fig. 12f and g, with the addition of Lysine, the intensity of blue emission at 440 nm enhanced gradually, while the peak at 624 nm remained unchanged, affording a robust ratiometric sensor toward lysine in a linear range of 0.5–260 μM with a detection limit of 94 nM. Furthermore, this probe was successfully applied to monitor the concentration variation of lysine inside living cells, which was meaningful for diagnosing various disease and disorders. Chen's group synthesized red dual-emissive CDs for selective, sensitive, rapid and accurate sensing of methyl blue in a fluorescence ratiometric method [143]. Upon addition of methyl blue, both the fluorescence intensity of R-CDs at 630 and 680 nm decreased. As a result, the ratios between the two emission intensities showed a good linear relationship within 0.5–300 μM, with a good correlation coefficient (R^2) of 0.997, and a detection limit as low as 0.43 μM. Such an interesting fluorescence quenching was due to energy transfer from R-CDs to methyl blue, which facilitated the non-radiative pathway and resulted in the PL diminishing for R-CDs. Very recently, taking advantage of optical properties and abundant surface functional groups of R-CDs [144], Lu's group fabricated the first ratiometric fluorescent platform for ultrasensitively quantifying organophosphorus pesticides (OPs) at approximately the pg L^{-1} level. The high recognition accuracy of this sensing platform to spiked samples obviously validated its practical applications in the field of food safety and environmental monitoring. In addition to the abovementioned analytes, R/NIR-CDs have shown great potential in the detection of temperature, hematin, moisture, tetracycline, alachlor herbicide, ziram, intracellular polarity, and even latent fingerprint [101,102,133,145–148].

4.3. Tumor therapy

Rapid early diagnosis and precise efficient therapy methods are of vital importance for prevention and treatment of cancer [29]. Among these anticancer models, R or NIR light-responsive nanotheranostics that integrate diagnosis and therapy into a single

nanoplatform have been widely used for cancer diagnosis and treatment owing to their unique non-invasiveness, non-destruction, real-time tracking, large tissue penetration depth, and low autofluorescence of tissues and mediums [22]. As a result, R/NIR-CDs are very appealing as nanotheranostic agent for anticancer applications, which involves photothermal therapy (PTT), photodynamic therapy (PDT), and targeted chemotherapy.

4.3.1. Photothermal therapy

As one of important modalities of treatment triggered by light, PTT can thermally ablate cancer cells through photothermal agents that controllably convert absorbed light to heat in targeted tumor area [15]. In this field, long wavelength emissive CDs have been utilized as PTT agent given their low phototoxicity, high photothermal conversion efficiency, and large tissue penetration depth. Ge's group prepared the first red fluorescent CDs with intrinsic theranostic properties through a simple hydrothermal approach [83]. The R-CDs displayed a broad absorption in a region from 400 to 750 nm with red emission centered at 640 nm, making them a promising agent for FL and PA imaging. More strikingly, under NIR light irradiation, the R-CDs showed a high photothermal conversion efficiency of 38.5%, allowing then to be used as PPT agents for photothermal cancer therapy. In Fig. 13a, under 671 nm laser excitation, the IR thermographic images of intratumorally injected mouse with R-CDs showed that the local tumor temperature can rapidly reach up to 58.4 °C within 10 min, which would cause irreversible damage to cells and tissues. With prolonged treatment, the mice reveled substantial empyrosis at the tumor areas and significant suppression of tumor growth, which were not achieved in the control group that administrated with saline (Fig. 13b and c). After 16 day, the dark burn scab detached from the skin, and the mice completely recovered without tumor reoccurrence. Meanwhile, the tissue slices analysis in Fig. 13d exhibited no obvious inflammation, cell necrosis, or apoptosis in the heart, liver, spleen, lung, and kidney, implying the absence of evident side effects. To further improve PTT effect for deep tumors, NIR-CDs have also been explored. For instance, Li and coworkers synthesized NIR-I absorbing CDs from watermelon with second near infrared (NIR-II) emission located in 900–1200 nm region [93]. Apart from NIR-II bioimaging, the NIR-CDs also performed well in photothermal

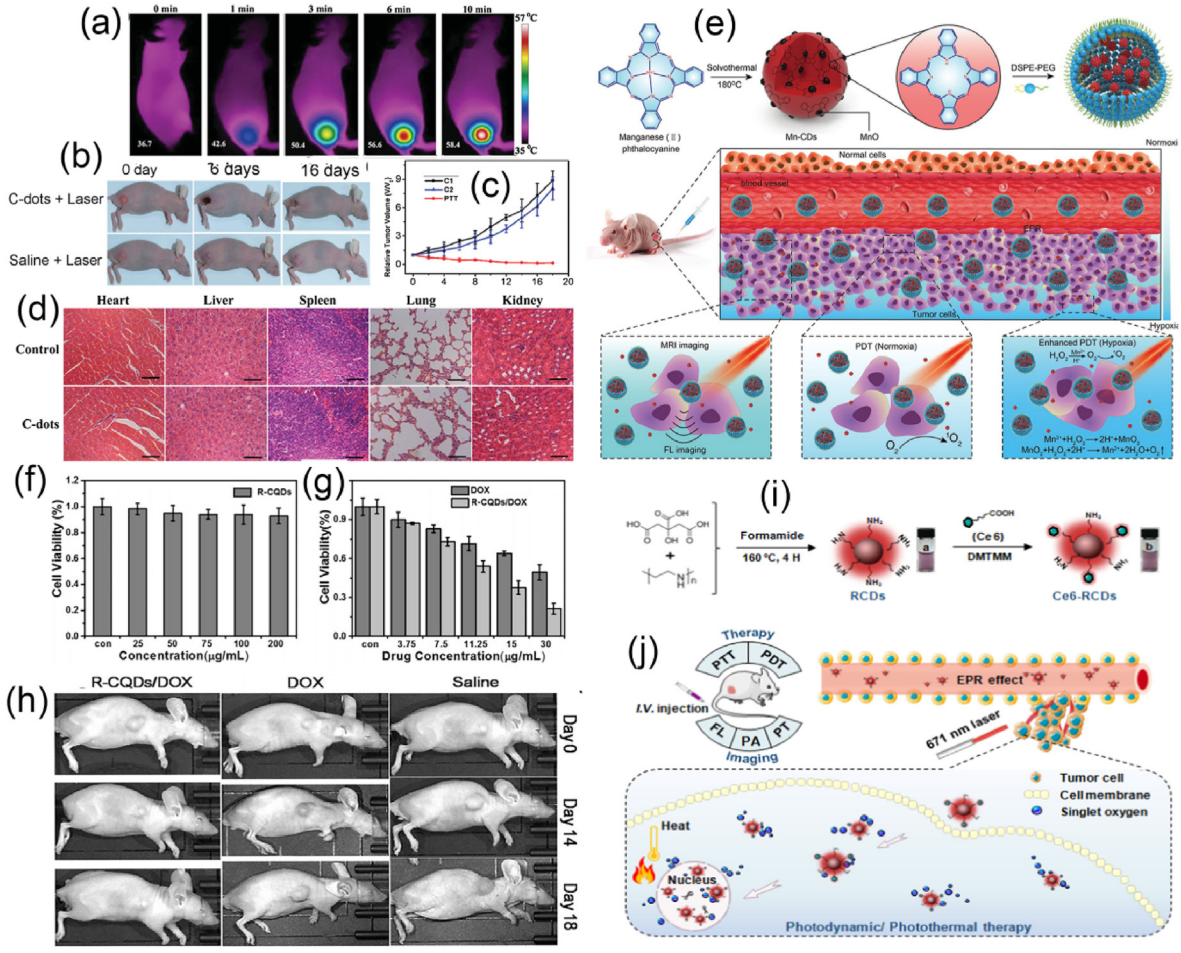

Fig. 13. (a) IR thermal imaging of intratumoral R-CDs injected mice tumor sites at different time points after irradiation by 671 nm laser at 2 W cm $^{-2}$; (b) photographs of the tumor-bearing mice on different days after different treatments; (c) relative change in the tumor volume of the tumor-bearing mice of the different groups after treatments; (d) hematoxylin and eosin (H&E)-stained slices of the heart, liver, spleen, lung, and kidney in mice after PTT. Scale bar is 50 μm. (e) Schematic diagram of the Mn-CD assembly as an acidic H_2O_2-driven oxygenerator to enhance the anticancer efficiency of PDT in a solid tumor. Reproduced with permission. (f and g) Cell viability of HeLa cells incubated with various concentrations of R-CQDs, DOX and R-CQDs/DOX; (h) photographs of the tumor-bearing mice on different days after various treatments, including those treated with saline solution, DOX, and DOX loaded-R-CQDs. (i) Schematic representation of the preparation of the R-CDs and Ce6-RCDs; (j) schematic illustration of the Ce6-RCDs for simultaneous FL, PA, and PT imaging and synergistic PTT/PDT process *in vivo*. Reprinted and adopted with permission from Refs. [56,82,84and144]. (Copyright 2015 and 2018 Wiley and Sons and Copyright 2019 and 2020 American Chemical Society).

cancer therapy due to their high photothermal conversion efficiency (30.6%). Under irradiation of 808 nm laser, the temperature of tumor tissues increased from 28 to 50 °C within 6 min after injection with NIR-CD solution, leading to the thermal ablating of cancer cells and subsequent disappearance of tumor. In addition, TP excited NIR-CDs also show great potential for PTT *in vitro* and *in vivo*. In 2017, Wang's group reported one kind of NIR-CDs with a comparable photothermal conversion efficiency to that of Au nanostructures (58.2%) [84], which was achieved by through co-doping S and Se elements into CDs via a hydrothermal method. Interestingly, these obtained NIR-CDs exhibited additional advantages, such as a wide absorption across the visible entire spectrum, maximum emissions at 731 and 820 nm, and a large TP absorption cross section (30,045 GM) at 880 nm. Based on these superior optical properties, NIR-CDs could be used as a promising multifunctional phototheranostic agents for simultaneously integrating TP excited FL imaging and highly efficient PTT of cancer cells *in vitro* and *in vivo*. The abovementioned examples highlights R/N-CDs as an excellent candidate for efficient cancer therapy. However, compared with the conventional PTT agents, the photothermal conversion efficiency of R/NIR-CDs requires further improvement to fulfill the requirements for clinic applications. As a consequence, the studies on NIR-responsive CDs with enhanced PTT performance and multifunctional theranostics are set to remain a crucial component of preclinical cancer research.

4.3.2. Photodynamic therapy

As the other kind of light-driven anticancer method, PDT exhibits numerous advantages over traditional cancer therapies (surgery, chemotherapy and radiotherapy), such as low drug resistance, trivial damage to marginal tissues, and mild side effects [82]. In PDT, photosensitizers, as one of the essential factors, can produce cytotoxic reactive oxygen through transferring energy to surrounding oxygen species (ROS), which destroys tumor cells under the excitation of a specific wavelength light. Up to now, a few examples of R/NIR-CDs were reported as potential PDT agents for various types of deep tumor tissues. Thereinto, a small part of R or NIR light-absorbing CDs possess an intrinsic capability of $^1O_2$ generation with QY varying from 1.3 to 62% [108,149–151], and can thus be directly utilized as PDT agents for multifunctional nanotheranostic applications. For instance, through the solvothermal treatment of manganese (II) phthalocyanine and subsequent self-assembly cooperated with DSPE-PEG [108], Ge's group developed a novel type of magnetofluorescent Mn-CDs with an efficient $^1O_2$ QY of 40% in ethanol, which also exhibited the merits of desirable physiological stability, intense NIR emission (745 nm), and T_1-weighted magnetic resonance (MR). More importantly, the Mn-CDs are capable of highly catalyzing H_2O_2 to generate oxygen in acidic solid tumors, so as to overcome the tumor hypoxia. With these collective properties, the Mn-CD assembly could be successfully used as agents for simultaneous bimodal FL/MR imaging and enhanced PDT (Fig. 13e). However, for the rest of most R/NIR-CDs, they are typically with low or no PDT functions, and require the introduction of additional photosensitizers to improve their PDT efficiency, which include boron dipyrromethene (BODIPY), cyanine dyes, porphyrin, chlorin and phthalocyanine derivatives, etc. [29]. For instance, Xie's group constructed R-CD-BODIPY nanocomposites (named as CBNPs) via the noncovalent interactions between them [152]. In this hybrid, the R-CDs acts as a donor and BODIPY as an acceptor chromophore, respectively, leading to the occurrence of FRET from R-CDs to attached BODIPY, which thereby endow CBNPs with a higher ability to generate singlet oxygen than that of R-CDs and BODIPY nanoparticles. *In vitro* cell experiments showed that CBNPs have the most profound phototoxicity effect, further confirming the improved PDT efficiency.

4.3.3. Targeted chemotherapy

R/NIR-CDs have an additional therapeutic potential as a promising class of drug carriers for efficient eradication of cancers due to their excellent optical property, large specific surface area, good biocompatibility, and low toxicity [98,153]. In comparison with free drug, nanodrug delivery systems built on R/NIR-CDs, especially those with specifically targeting function, are expected to achieve improved drug solubility, extended tumor retention period, enhanced therapeutic efficiency, and reduced side effects. For instance, Fan's group constructed a nanocomposite of red-emissive carbon quantum dots/doxorubicin (R-CQDs/DOX) through the π-π stacking interactions [81], which possess a capacity to enter into the nuclei of both cancer cells and cancer stem cells. In the following cytotoxicity evaluation, it was found that, after culturing with the same concentration of DOX (30 μg/mL) for 12 h, the average cell viability of HeLa cells treated with R-CQDs/DOX is approximately 21%, much lower than that treated with free DOX, indicating the enhanced effectiveness for killing HeLa cells (Fig. 13f and g). Correspondingly, *in vivo* experiments reveal the intravenously injected R-CQDs/DOX can dramatically inhibit tumor growth without obvious side effects, whereas the control groups treated with DOX and saline solution exhibit an evident increment in tumor size over the course of treatment (Fig. 13h). As a further study, the same group recently developed a versatile strategy for constructing N-CDs-based anticancer drug carriers for targeted tumor theranostics in mice [100]. In this platform, the multiple paired α-carboxyl and amino groups attached on NIR-CD surfaces performed a beneficial role in two ways. On the one hand, these functional groups could trigger a multivalent, strong interaction with the large neutral amino acid transporter 1 overexpressed in most tumors, consequently leading to the tumor-specific targeting property of NIR-CDs, regardless of the origin or stemness. On the other hand, these functional groups enabled the loading of topotecan hydrochloride (TPTC) through π−π stacking interactions. Coupled with the additional properties of minimal toxicity, intrinsic imaging capacity, and intrinsic ability to penetrate the blood−brain barrier, the NIR-CDs were successfully applied as multifunctional nanoplatforms for selectively imaging and efficiently delivering therapeutic agents to various tumors and diseases in the central nervous system. Those results indicate that R/NIR-CDs can effectively deliver aromatic chemotherapy drugs, resulting in enhanced therapeutic efficacy to cancers as compared to that of free drugs.

4.3.4. Synergistic therapy

Although PTT and PDT exhibit many advantages for anticancer treatment, each technique suffers from inherent drawbacks, such as the potential tissue damage due to high-power laser irradiation, and the limited efficacy due to the hypoxia nature inside tumors, which can severely impede their therapeutic efficacy [29]. Hence, to meet high therapeutic requirements, great efforts have been devoted to producing R/NIR-CDs with the simultaneous photothermal and photodynamic effects, which could be used in synergistic therapy that integrates the advantages of PTT and PDT [21]. For example, Jia et al. demonstrated that hypocrella bambusae-derived R-CDs can be used as cancer theragnostic for simultaneous imaging-based PTT and PDT [150], with a high photothermal conversion efficiency of 27.6% and an impressive $^1O_2$ generation efficiency of 38% under 635 nm laser irradiation. Lin's group loaded a small amount of photosensitizer chlorin e6 (Ce6) (0.56% of mass) onto amino-rich R-CDs for synergistic PTT/PDT against cancer triggered by a single 671 nm laser, as shown in Fig. 13i and j [55]. The obtained Ce6-RCDs provide a stronger anticancer effect upon a low power density of laser (0.50 W cm^{-2}) than the equivalent Ce6 or R-CDs under the same irradiation conditions. Although R/NIR-CDs have attractive applications in phototherapy and

chemotherapy, it is important to note that there are still few reports of R/NIR-CDs with these fascinating features. In addition, most of the previously reported R/NIR-CDs are subjected to nonselective interactions with both tumor cells and normal cells [100]. As a result, how to synthesize smart R/NIR-CDs-based nanohybrids with specific targeting function, multimodal bioimaging functions, and multiple therapeutic functions is also a research hotspot in biomedical applications of CDs.

5. Conclusions and perspectives

In this review, we summarized the recent research progress of R/NIR-CDs about their raw materials, synthetic routes and optical properties, involving the effects of particle size, surface states, heteroatom doping, pH, solvent, concentration, and even aggregation on their PL regulation. Significantly, the intriguing merits of R/NIR-CDs are also highlighted in their applications for both *in vitro* and *in vivo* bioimaging including FL and PA imaging, biosensing, cancer therapy including photodynamic therapy, photothermal therapy, chemotherapy, and synergistic therapy. Although the related studies regarding the synthesis and biomedical applications of R/NIR-CDs have realized rapid growth within a short time, those reported R/NIR-CDs are facing great challenges in practical applications as stated below.

Firstly, the synthesis of R/NIR-CDs should be green, scalable, reproducible, and low-cost. But till now, most of the reported R/NIR-CDs are produced from expensive, even poisonous chemical reagents via time-consuming or energy-intensive approaches, as well as complicated and inefficient purification techniques, which hinder their practical applications. Therefore, the effective combination of biomass synthesis and sustainable synthesis technology as well as fast purification methods is the future direction for the green and massive synthesis of R/NIR-CDs. In addition, the proposed explanations of luminescence mechanism of R/NIR-CDs are not comprehensive enough, which typically different from each other, highly depending on particle size, surface states, heteroatom doping, or combined effects from the three factors above. Therefore, it is imperative for researchers to explore luminescence mechanisms of R/NIR-CDs through *in situ* characterizing their structural components with advanced technique and rationally simulating the possible luminescence process with theoretical calculation, which is expected to guide the regulation of optical properties of CDs.

Secondly, NIR-II (900–1500 nm) light excited and emissive CDs with high QY in aqueous solution are highly desired for *in vivo* applications, especially bioimaging and phototherapy, owing to their minimal photodamage and tissue absorption, negligible interference from autofluorescence to biological tissues, and deep tissue penetration. Nevertheless, up to now, research work acquired NIR-I (600–900 nm) light emitting CDs with low QY in aqueous solution under excitation of visible light. To this end, more in-depth researches should be carried out, which include concertedly choosing proper precursors and synthetic methods. Moreover, much attention should be switched from the low toxicity and good biocompatibility of R/NIR-CDs to their interactions with biomacromolecules, including molecular interaction mechanisms, biological effects, stability in different circumstances, and long-term biosafety.

Thirdly, despite remarkable progress in the synthesis of R/NIR-CDs and application in sensing, their sensitivity and selectivity toward specific analytes are limited when compared with other probes, which is due to abundant diversity of surface functional groups and defects on CD surfaces. In order to improve the sensing capability, at least one kind of substance that provides selectivity for analytes of interest, can be mixed with other carbon precursors for the preparation of functional R/NIR-CDs based on our experiences. In this case, the molar ratio of the selected precursors, reaction conditions, reaction mediums, as well as subsequent separation techniques have to be investigated carefully. For cancer therapy, developing multifunctional NIR-CD-based nanotheranostics with a multimodal imaging-guided synergistic therapy has practical importance, which could maximize the theranostic effects reasonably, and provide precise diagnosis and treatment of cancers. At the same time, to improve cancer treatment efficacy and simultaneously reduce the side effects, the tumor microenvironment-mediated response, such as pH, hypoxia, temperature, etc., should be utilized in R/NIR-CD-based nanomedicine combined with the receptor-mediated targeting strategy. Besides cancer therapy, research on the biomedical application of R/NIR-CDs in other diseases should be paid considerable attention, which include cardiovascular, cerebrovascular, wound-healing, and respiratory system diseases.

With the above efforts, it is expected that booming R/NIR-CDs will promote their applications in bioimaging, biosensing and biotherapy, and open new perspectives toward design and synthesis of biocompatible CDs to meet the requirements of clinical applications.

Declaration of competing interest

The authors declare no conflict of interest.

Acknowledgements

The authors acknowledge financial support from the National Natural Science Foundation of China (51803233, 21771039 and 21975048), China Postdoctoral Science Foundation (2019M651999), and the Shanghai Science and Technology Committee (19DZ2270100).

References

[1] S.Y. Lim, W. Shen, Z. Gao, Carbon quantum dots and their applications, Chem. Soc. Rev. 44 (1) (2015) 362–381.
[2] M. Shamsipur, A. Barati, S. Karami, Long-wavelength, multicolor, and white-light emitting carbon-based dots: achievements made, challenges remaining, and applications, Carbon 124 (2017) 429–472.
[3] M. Semeniuk, Z. Yi, V. Poursorkhabi, J. Tjong, S. Jaffer, Z.H. Lu, et al., Future perspectives and review on organic carbon dots in electronic applications, ACS Nano 13 (6) (2019) 6224–6255.
[4] C. Xia, S. Zhu, T. Feng, M. Yang, B. Yang, Evolution and synthesis of carbon dots: from carbon dots to carbonized polymer dots, Adv. Sci. 6 (23) (2019) 1901316.
[5] M.L. Liu, B.B. Chen, C.M. Li, C.Z. Huang, Carbon dots: synthesis, formation mechanism, fluorescence origin and sensing applications, Green Chem. 21 (3) (2019) 449–471.
[6] J. Gao, M. Zhu, H. Huang, Y. Liu, Z. Kang, Advances, challenges and promises of carbon dots, Inorg. Chem. Front. 4 (12) (2017) 1963–1986.
[7] L. Li, T. Dong, Photoluminescence tuning in carbon dots: surface passivation or/and functionalization, heteroatom doping, J. Mater. Chem. C 6 (30) (2018) 7944–7970.
[8] Y. Zhou, K.J. Mintz, S.K. Sharma, R.M. Leblanc, Carbon dots: diverse preparation, application, and perspective in surface chemistry, Langmuir 35 (28) (2019) 9115–9132.
[9] Z. Li, L. Wang, Y. Li, Y. Feng, W. Feng, Frontiers in carbon dots: design, properties and applications, Mater. Chem. Front. 3 (12) (2019) 2571–2601.
[10] S. Tao, S. Zhu, T. Feng, C. Xia, Y. Song, B. Yang, The polymeric characteristics and photoluminescence mechanism in polymer carbon dots: a review, Mater. Today Chem. 6 (2017) 13–25.
[11] M. Han, S.J. Zhu, S.Y. Lu, Y.B. Song, T.L. Feng, S.Y. Tao, et al., Recent progress on the photocatalysis of carbon dots: classification, mechanism and applications, Nano Today 19 (2018) 201–218.
[12] Z. Kang, S.-T. Lee, Carbon dots: advances in nanocarbon applications, Nanoscale 11 (41) (2019) 19214–19224.
[13] L. Xiao, H. Sun, Novel properties and applications of carbon nanodots, Nanoscale Horiz 3 (6) (2018) 565–597.
[14] Z. Fan, S. Li, F. Yuan, L. Fan, Fluorescent graphene quantum dots for biosensing and bioimaging, RSC Adv. 5 (25) (2015) 19773–19789.

[15] X. Shi, H. Meng, Y. Sun, L. Qu, Y. Lin, Z. Li, et al., Far-red to near-infrared carbon dots: preparation and applications in biotechnology, Small 15 (48) (2019), e1901507.
[16] X.T. Zheng, A. Ananthanarayanan, K.Q. Luo, P. Chen, Glowing graphene quantum dots and carbon dots: properties, syntheses, and biological applications, Small 11 (14) (2015) 1620–1636.
[17] B. Yao, H. Huang, Y. Liu, Z. Kang, Carbon dots: a small conundrum, Trends in Chemistry 1 (2) (2019) 235–246.
[18] D. Xu, Q. Lin, H.T. Chang, Recent advances and sensing applications of carbon dots, Small Methods 4 (4) (2020) 1900387.
[19] P. Miao, K. Han, Y. Tang, B. Wang, T. Lin, W. Cheng, Recent advances in carbon nanodots: synthesis, properties and biomedical applications, Nanoscale 7 (5) (2015) 1586–1595.
[20] D. Gao, H. Zhao, X. Chen, H. Fan, Recent advance in red-emissive carbon dots and their photoluminescent mechanisms, Mater. Today Chem. 9 (2018) 103–113.
[21] Z.J. Zhu, Y.L. Zhai, Z.H. Li, P.Y. Zhu, S. Mao, C.Z. Zhu, et al., Red carbon dots: optical property regulations and applications, Mater, Today Off. 30 (2019) 52–79.
[22] W. Su, H. Wu, H. Xu, Y. Zhang, Y. Li, X. Li, et al., Carbon dots: a booming material for biomedical applications, Mater. Chem. Front. 4 (3) (2020) 821–836.
[23] W. Liu, C. Li, Y. Ren, X. Sun, W. Pan, Y. Li, et al., Carbon dots: surface engineering and applications, J. Mater. Chem. B 4 (35) (2016) 5772–5788.
[24] B. Zhou, Z. Guo, Z. Lin, L. Zhang, B.-P. Jiang, X.-C. Shen, Recent insights into near-infrared light-responsive carbon dots for bioimaging and cancer phototherapy, Inorg. Chem. Front. 6 (5) (2019) 1116–1128.
[25] H. Jia, Z. Wang, T. Yuan, F. Yuan, X. Li, Y. Li, et al., Electroluminescent warm white light-emitting diodes based on passivation enabled bright red bandgap emission carbon quantum dots, Adv. Sci. 6 (2019) 1900397, 0.
[26] S. Anwar, H. Ding, M. Xu, X. Hu, Z. Li, J. Wang, et al., Recent advances in synthesis, optical properties, and biomedical applications of carbon dots, ACS Appl. Nano Mater 2 (6) (2019) 2317–2338.
[27] J. Wang, Y. Zhu, L. Wang, Synthesis and applications of red-emissive carbon dots, Chem. Rec. 19 (10) (2019) 2083–2094.
[28] S. Zhu, Y. Song, J. Wang, H. Wan, Y. Zhang, Y. Ning, et al., Photoluminescence mechanism in graphene quantum dots: quantum confinement effect and surface/edge state, Nano Today 13 (2017) 10–14.
[29] Q.Y. Jia, Z.Y. Zhao, K. Liang, F.C. Nan, Y. Li, J. Wang, et al., Recent advances and prospects of carbon dots in cancer nanotheranostics, Mater. Chem. Front. 4 (2) (2020) 449–471.
[30] P. He, Y. Shi, T. Meng, T. Yuan, Y. Li, X. Li, et al., Recent advances in white light-emitting diodes of carbon quantum dots, Nanoscale 12 (8) (2020) 4826–4832.
[31] J. Du, N. Xu, J. Fan, W. Sun, X. Peng, Carbon dots for in vivo bioimaging and theranostics, Small 15 (32) (2019), e1805087.
[32] M. Pirsaheb, S. Mohammadi, A. Salimi, Current advances of carbon dots based biosensors for tumor marker detection, cancer cells analysis and bioimaging, TrAC Trends Anal. Chem. (Reference Ed.) 115 (2019) 83–99.
[33] H. Ding, S.B. Yu, J.S. Wei, H.M. Xiong, Full-color light-emitting carbon dots with a surface-state-controlled luminescence mechanism, ACS Nano 10 (1) (2016) 484–491.
[34] M. Li, T. Chen, J.J. Gooding, J. Liu, Review of carbon and graphene quantum dots for sensing, ACS Sens. 4 (7) (2019) 1732–1748.
[35] X. Hai, J. Feng, X. Chen, J. Wang, Tuning the optical properties of graphene quantum dots for biosensing and bioimaging, J. Mater. Chem. B 6 (20) (2018) 3219–3234.
[36] T. Yuan, T. Meng, P. He, Y.X. Shi, Y.C. Li, X.H. Li, et al., Carbon quantum dots: an emerging material for optoelectronic applications, J. Mater. Chem. C 7 (23) (2019) 6820–6835.
[37] L. Sciortino, A. Sciortino, R. Popescu, R. Schneider, D. Gerthsen, S. Agnello, et al., Tailoring the emission color of carbon dots through nitrogen-induced changes of their crystalline structure, J. Phys. Chem. C 122 (34) (2018) 19897–19903.
[38] M. Sun, C. Liang, Z. Tian, E.V. Ushakova, D. Li, G. Xing, et al., Realization of the photostable intrinsic core emission from carbon dots through surface deoxidation by ultraviolet irradiation, J. Phys. Chem. Lett. 10 (11) (2019) 3094–3100.
[39] A. Zhao, Z. Chen, C. Zhao, N. Gao, J. Ren, X. Qu, Recent advances in bioapplications of C-dots, Carbon 85 (2015) 309–327, 0.
[40] F. Li, D. Yang, H. Xu, Non-metal-heteroatom-doped carbon dots: synthesis and properties, Chem. Eur J. 25 (5) (2019) 1165–1176.
[41] H. Xu, Q. Li, L. Wang, Y. He, J. Shi, B. Tang, et al., Nanoscale optical probes for cellular imaging, Chem. Soc. Rev. 43 (8) (2014) 2650.
[42] H.Y. Ko, Y.W. Chang, G. Paramasivam, M.S. Jeong, S. Cho, S. Kim, In vivo imaging of tumour bearing near-infrared fluorescence-emitting carbon nanodots derived from tire soot, Chem. Commun. 49 (87) (2013) 10290–10292.
[43] X. Tan, Y. Li, X. Li, S. Zhou, L. Fan, S. Yang, Electrochemical synthesis of small-sized red fluorescent graphene quantum dots as a bioimaging platform, Chem. Commun. 51 (13) (2015) 2544–2546.
[44] L. Bao, C. Liu, Z.L. Zhang, D.W. Pang, Photoluminescence-tunable carbon nanodots: surface-state energy-gap tuning, Adv. Mater. 27 (10) (2015) 1663–1667.
[45] C.-C. Ke, Y.-C. Yang, W.-L. Tseng, Synthesis of blue-, green-, yellow-, and red-emitting graphene-quantum-dot-based nanomaterials with excitation-independent emission, part. Part, Syst. Charact. 33 (3) (2016) 132–139.
[46] X. Meng, Q. Chang, C. Xue, J. Yang, S. Hu, Full-colour carbon dots from energy-efficient synthesis to concentration-dependent photoluminescence properties, Chem. Commun. 53 (21) (2017) 3074–3077.
[47] D. Qu, Z. Sun, The formation mechanism and fluorophores of carbon dots synthesized via a bottom-up route, Mater. Chem. Front. 4 (2) (2020) 400–420.
[48] S. Sarkar, M. Sudolská, M. Dubecký, C.J. Reckmeier, A.L. Rogach, R. Zbořil, et al., Graphitic nitrogen doping in carbon dots causes red-shifted absorption, J. Phys. Chem. C 120 (2) (2016) 1303–1308.
[49] E.V. Kundelev, N.V. Tepliakov, M.Y. Leonov, V.G. Maslov, A.V. Baranov, A.V. Fedorov, et al., Amino functionalization of carbon dots leads to red emission enhancement, J. Phys. Chem. Lett. 10 (17) (2019) 5111–5116.
[50] J. Manioudakis, F. Victoria, C.A. Thompson, L. Brown, M. Movsum, R. Lucifero, et al., Effects of nitrogen-doping on the photophysical properties of carbon dots, J. Mater. Chem. C 7 (4) (2019) 853–862.
[51] S. Qu, D. Zhou, D. Li, W. Ji, P. Jing, D. Han, et al., Toward efficient orange emissive carbon nanodots through conjugated sp(2) -domain controlling and surface charges engineering, Adv. Mater. 28 (18) (2016) 3516–3521.
[52] L. Pan, S. Sun, A. Zhang, K. Jiang, L. Zhang, C. Dong, et al., Truly fluorescent excitation-dependent carbon dots and their applications in multicolor cellular imaging and multidimensional sensing, Adv. Mater. 27 (47) (2015) 7782–7787.
[53] H. Ding, J.-S. Wei, N. Zhong, Q.-Y. Gao, H.-M. Xiong, Highly efficient red-emitting carbon dots with gram-scale yield for bioimaging, Langmuir 33 (44) (2017) 12635–12642.
[54] X. Miao, D. Qu, D. Yang, B. Nie, Y. Zhao, H. Fan, et al., Synthesis of carbon dots with multiple color emission by controlled graphitization and surface functionalization, Adv. Mater. 30 (1) (2018) 1704740.
[55] S. Sun, J. Chen, K. Jiang, Z. Tang, Y. Wang, Z. Li, et al., Ce6-Modified carbon dots for multimodal-imaging-guided and single-NIR-laser-triggered photothermal/photodynamic synergistic cancer therapy by reduced irradiation power, ACS Appl. Mater. Interfaces 11 (6) (2019) 5791–5803.
[56] T. Feng, Q. Zeng, S. Lu, X. Yan, J. Liu, S. Tao, et al., Color-tunable carbon dots possessing solid-state emission for full-color light-emitting diodes applications, ACS Photonics 5 (2) (2017) 502–510.
[57] W. Gao, H. Song, X. Wang, X. Liu, X. Pang, Y. Zhou, et al., Carbon dots with red emission for sensing of Pt2+, Au3+, and Pd2+ and their bioapplications in vitro and in vivo, ACS Appl. Mater. Interfaces 10 (1) (2017) 1147–1154.
[58] T. Zhang, F. Zhao, L. Li, B. Qi, D. Zhu, J. Lu, et al., Tricolor white-light-emitting carbon dots with multiple-Cores@Shell structure for WLED application, ACS Appl. Mater. Interfaces 10 (23) (2018) 19796–19805.
[59] F. Yan, Y. Jiang, X. Sun, J. Wei, L. Chen, Y. Zhang, Multicolor carbon dots with concentration-tunable fluorescence and solvent-affected aggregation states for white light-emitting diodes, Nano Res 13 (1) (2019) 52–60.
[60] L. Pan, S. Sun, L. Zhang, K. Jiang, H. Lin, Near-infrared emissive carbon dots for two-photon fluorescence bioimaging, Nanoscale 8 (39) (2016) 17350–17356.
[61] F. Arcudi, L. Đorđević, M. Prato, Rationally designed carbon nanodots towards pure white-light emission, Angew. Chem. Int. Ed. 56 (15) (2017) 4170–4173.
[62] H. Ding, J.S. Wei, P. Zhang, Z.Y. Zhou, Q.Y. Gao, H.M. Xiong, Solvent-controlled synthesis of highly luminescent carbon dots with a wide color gamut and narrowed emission peak widths, Small 14 (22) (2018), e1800612.
[63] M.R. Zhang, R.G. Su, J. Zhong, L. Fei, W. Cai, Q.W. Guan, et al., Red/orange dual-emissive carbon dots for pH sensing and cell imaging, Nano Res 12 (4) (2019) 815–821.
[64] S.K. Bhunia, A. Saha, A.R. Maity, S.C. Ray, N.R. Jana, Carbon nanoparticle-based fluorescent bioimaging probes, Sci. Rep. 3 (2013) 1473.
[65] H. Ali, S.K. Bhunia, C. Dalal, N.R. Jana, Red fluorescent carbon nanoparticle-based cell imaging probe, ACS Appl. Mater. Interfaces 8 (14) (2016) 9305–9313.
[66] V. Gude, A. Das, T. Chatterjee, P.K. Mandal, Molecular origin of photoluminescence of carbon dots: aggregation-induced orange-red emission, Phys. Chem. Chem. Phys. 18 (40) (2016) 28274–28280.
[67] J. Shao, S. Zhu, H. Liu, Y. Song, S. Tao, B. Yang, Full-color emission polymer carbon dots with quench-resistant solid-state fluorescence, Adv. Sci. 4 (12) (2017) 1700395.
[68] J. Bai, Y. Ma, G. Yuan, X. Chen, J. Mei, L. Zhang, et al., Solvent-controlled and solvent-dependent strategies for the synthesis of multicolor carbon dots for pH sensing and cell imaging, J. Mater. Chem. C 7 (31) (2019) 9709–9718.
[69] X. Li, Z. Wang, Y. Liu, W. Zhang, C. Zhu, X. Meng, Bright tricolor ultrabroadband emission carbon dots for white light-emitting diodes with a 96.5 high color rendering index, J. Mater. Chem. C 8 (4) (2020) 1286–1291.
[70] K. Zheng, X. Li, M. Chen, Y. Gong, A. Tang, Z. Wang, et al., Controllable synthesis highly efficient red, yellow and blue carbon nanodots for photoluminescent light-emitting devices, Chem. Eng. J. 380 (2020) 122503.
[71] K. Yuan, X.H. Zhang, R.H. Qin, X.F. Ji, Y.H. Cheng, L.L. Li, et al., Surface state modulation of red emitting carbon dots for white light-emitting diodes, J. Mater. Chem. C 6 (46) (2018) 12631–12637.
[72] F. Yuan, S. Li, Z. Fan, X. Meng, L. Fan, S. Yang, Shining carbon dots: synthesis and biomedical and optoelectronic applications, Nano Today 11 (5) (2016) 565–586.
[73] F. Arcudi, L. Dordevic, M. Prato, Design, synthesis, and functionalization strategies of tailored carbon nanodots, Acc. Chem. Res. 52 (8) (2019)

2070–2079.
[74] S. Lu, L. Sui, J. Liu, S. Zhu, A. Chen, M. Jin, et al., Near-infrared photoluminescent polymer-carbon nanodots with two-photon fluorescence, Adv. Mater. 29 (15) (2017) 1603443.
[75] K.K. Liu, S.Y. Song, L.Z. Sui, S.X. Wu, P.T. Jing, R.Q. Wang, et al., Efficient red/near-infrared-emissive carbon nanodots with multiphoton excited upconversion fluorescence, Adv. Sci. 6 (17) (2019) 1900766.
[76] K. Jiang, S. Sun, L. Zhang, Y. Lu, A. Wu, C. Cai, et al., Red, green, and blue luminescence by carbon dots: full-color emission tuning and multicolor cellular imaging, Angew. Chem. Int. Ed. 54 (18) (2015) 5360–5363.
[77] J. Liu, D. Li, K. Zhang, M. Yang, H. Sun, B. Yang, One-step hydrothermal synthesis of nitrogen-doped conjugated carbonized polymer dots with 31% efficient red emission for in vivo imaging, Small 14 (15) (2018), e1703919.
[78] X. Ye, Y. Xiang, Q. Wang, Z. Li, Z. Liu, A red emissive two-photon fluorescence probe based on carbon dots for intracellular pH detection, Small 15 (48) (2019), e1901673.
[79] F. Yuan, T. Yuan, L. Sui, Z. Wang, Z. Xi, Y. Li, et al., Engineering triangular carbon quantum dots with unprecedented narrow bandwidth emission for multicolored LEDs, Nat. Commun. 9 (1) (2018) 2249.
[80] S. Ghosh, H. Ali, N.R. Jana, Water dispersible red fluorescent carbon nanoparticles via carbonization of resorcinol, Acs Sustain Chem. Eng. 7 (14) (2019) 12629–12637.
[81] W. Su, R. Guo, F. Yuan, Y. Li, X. Li, Y. Zhang, et al., Red-emissive carbon quantum dots for nuclear drug delivery in cancer stem cells, J. Phys. Chem. Lett. 11 (4) (2020) 1357–1363.
[82] J. Ge, M. Lan, B. Zhou, W. Liu, L. Guo, H. Wang, et al., A graphene quantum dot photodynamic therapy agent with high singlet oxygen generation, Nat. Commun. 5 (2014) 4596.
[83] J. Ge, Q. Jia, W. Liu, L. Guo, Q. Liu, M. Lan, et al., Red-emissive carbon dots for fluorescent, photoacoustic, and thermal theranostics in living mice, Adv. Mater. 27 (28) (2015) 4169–4177.
[84] M. Lan, S. Zhao, Z. Zhang, L. Yan, L. Guo, G. Niu, et al., Two-photon-excited near-infrared emissive carbon dots as multifunctional agents for fluorescence imaging and photothermal therapy, Nano Res 10 (9) (2017) 3113–3123.
[85] D. Huang, H. Zhou, Y. Wu, T. Wang, L. Sun, P. Gao, et al., Bottom-up synthesis and structural design strategy for graphene quantum dots with tunable emission to the near infrared region, Carbon 142 (2019) 673–684.
[86] Z. Wang, F. Yuan, X. Li, Y. Li, H. Zhong, L. Fan, et al., 53% efficient red emissive carbon quantum dots for high color rendering and stable warm white-light-emitting diodes, Adv. Mater. 29 (37) (2017) 1702910.
[87] J. Zhan, B. Geng, K. Wu, G. Xu, L. Wang, R. Guo, et al., A solvent-engineered molecule fusion strategy for rational synthesis of carbon quantum dots with multicolor bandgap fluorescence, Carbon 130 (2018) 153–163.
[88] B. Yuan, S. Guan, X. Sun, X. Li, H. Zeng, Z. Xie, et al., Highly efficient carbon dots with reversibly switchable green-red emissions for trichromatic white light-emitting diodes, ACS Appl. Mater. Interfaces 10 (18) (2018) 16005–16014.
[89] S.-M. Wei, K. Feng, C. Li, N. Xie, Y. Wang, X.-L. Yang, et al., ZnCl2 enabled synthesis of highly crystalline and emissive carbon dots with exceptional capability to generate O2•−, Matter 2 (2) (2020) 495–506.
[90] L.P. Li, R.P. Zhang, C.X. Lu, J.H. Sun, L.J. Wang, B.T. Qu, et al., In situ synthesis of NIR-light emitting carbon dots derived from spinach for bio-imaging applications, J. Mater. Chem. B 5 (35) (2017) 7328–7334.
[91] H. Ding, Y. Ji, J.-S. Wei, Q.-Y. Gao, Z.-Y. Zhou, H.-M. Xiong, Facile synthesis of red-emitting carbon dots from pulp-free lemon juice for bioimaging, J. Mater. Chem. B 5 (26) (2017) 5272–5277.
[92] A. Bhati, S.R. Anand, Gunture, A.K. Garg, P. Khare, S.K. Sonkar, Sunlight-induced photocatalytic degradation of pollutant dye by highly fluorescent red-emitting Mg-N-embedded carbon dots, Acs Sustain Chem. Eng. 6 (7) (2018) 9246–9256.
[93] Y. Li, G. Bai, S. Zeng, J. Hao, Theranostic carbon dots with innovative NIR-II emission for in vivo renal-excreted optical imaging and photothermal therapy, ACS Appl. Mater. Interfaces 11 (5) (2019) 4737–4744.
[94] K. Hola, M. Sudolska, S. Kalytchuk, D. Nachtigallova, A.L. Rogach, M. Otyepka, et al., Graphitic nitrogen triggers red fluorescence in carbon dots, ACS Nano 11 (12) (2017) 12402–12410.
[95] L. Jiang, H. Ding, M. Xu, X. Hu, S. Li, M. Zhang, et al., UV-Vis-NIR full-range responsive carbon dots with large multiphoton absorption cross sections and deep-red fluorescence at nucleoli and in vivo, Small 16 (19) (2020), e2000680.
[96] D. Li, P. Jing, L. Sun, Y. An, X. Shan, X. Lu, et al., Near-infrared excitation/emission and multiphoton-induced fluorescence of carbon dots, Adv. Mater. 30 (13) (2018) 1705913.
[97] C.L. Shen, Q. Lou, J.H. Zang, K.K. Liu, S.N. Qu, L. Dong, et al., Near-infrared chemiluminescent carbon nanodots and their application in reactive oxygen species bioimaging, Adv. Sci. 7 (8) (2020) 1903525.
[98] X. Miao, X. Yan, D. Qu, D. Li, F.F. Tao, Z. Sun, Red emissive sulfur, nitrogen codoped carbon dots and their application in ion detection and theraonostics, ACS Appl. Mater. Interfaces 9 (22) (2017) 18549–18556.
[99] F. Yuan, Z. Wang, X. Li, Y. Li, Z.a. Tan, L. Fan, et al., Bright multicolor bandgap fluorescent carbon quantum dots for electroluminescent light-emitting diodes, Adv. Mater. 29 (3) (2017) 1604436.
[100] S. Li, W. Su, H. Wu, T. Yuan, C. Yuan, J. Liu, et al., Targeted tumour theranostics in mice via carbon quantum dots structurally mimicking large amino acids, Nature Biomedical Engineering (2020), https://doi.org/10.1038/s41551-020-0540-y.
[101] J. Chen, J.-S. Wei, P. Zhang, X.-Q. Niu, W. Zhao, Z.-Y. Zhu, et al., Red-emissive carbon dots for fingerprints detection by spray method: coffee ring effect and unquenched fluorescence in drying process, ACS Appl. Mater. Interfaces 9 (22) (2017) 18429–18433.
[102] G.C. Zuo, Y.Z. Jiao, R.R. Gao, A.M. Xie, X.H. Pan, T. Su, et al., Lipophilic red-emitting oligomeric organic dots for moisture detection and cell imaging, ACS Appl. Nano Mater. 3 (2) (2020) 1942–1949.
[103] Y. Liu, H. Gou, X. Huang, G. Zhang, K. Xi, X. Jia, Rational synthesis of highly efficient ultra-narrow red-emitting carbon quantum dots for NIR-II two-photon bioimaging, Nanoscale 12 (3) (2020) 1589–1601.
[104] F.L. Yuan, P. He, Z.F. Xi, X.H. Li, Y.C. Li, H.Z. Zhong, et al., Highly efficient and stable white LEDs based on pure red narrow bandwidth emission triangular carbon quantum dots for wide-color gamut backlight displays, Nano Res 12 (7) (2019) 1669–1674.
[105] Q. Wang, S.J. Zhang, B.Y. Wang, X.Y. Yang, B. Zou, B. Yang, et al., Pressure-triggered aggregation-induced emission enhancement in red emissive amorphous carbon dots, Nanoscale Horiz 4 (5) (2019) 1227–1231.
[106] Z. Han, K. Wang, F. Du, Z. Yin, Z. Xie, S. Zhou, High efficiency red emission carbon dots based on phenylene diisocyanate for trichromatic white and red LEDs, J. Mater. Chem. C 6 (36) (2018) 9631–9635.
[107] J. Liu, Y. Geng, D. Li, H. Yao, Z. Huo, Y. Li, et al., Deep red emissive carbonized polymer dots with unprecedented narrow full width at half maximum, Adv. Mater. 32 (17) (2020), e1906641.
[108] Q. Jia, J. Ge, W. Liu, X. Zheng, S. Chen, Y. Wen, et al., A magnetofluorescent carbon dot assembly as an acidic H2 O2 -driven oxygenerator to regulate tumor hypoxia for simultaneous bimodal imaging and enhanced photodynamic therapy, Adv. Mater. 30 (13) (2018), e1706090.
[109] M. Zheng, Y. Li, S. Liu, W. Wang, Z. Xie, X. Jing, One-pot to synthesize multifunctional carbon dots for near infrared fluorescence imaging and photothermal cancer therapy, ACS Appl. Mater. Interfaces 8 (36) (2016) 23533–23541.
[110] Z. Tian, X. Zhang, D. Li, D. Zhou, P. Jing, D. Shen, et al., Full-color inorganic carbon dot phosphors for white-light-emitting diodes, Adv. Opt. Mat. 5 (19) (2017) 1700416.
[111] J. Zhu, X. Bai, X. Chen, H. Shao, Y. Zhai, G. Pan, et al., Spectrally tunable solid state fluorescence and room-temperature phosphorescence of carbon dots synthesized via seeded growth method, Adv. Opt. Mat. 7 (9) (2019) 1801599.
[112] M.A. Sk, A. Ananthanarayanan, L. Huang, K.H. Lim, P. Chen, Revealing the tunable photoluminescence properties of graphene quantum dots, J. Mater. Chem. C 2 (34) (2014) 6954–6960.
[113] Y. Xu, M. Wu, Y. Liu, X.Z. Feng, X.B. Yin, X.W. He, et al., Nitrogen-doped carbon dots: a facile and general preparation method, photoluminescence investigation, and imaging applications, Chem. Eur J. 19 (7) (2013) 2276–2283.
[114] M. Zheng, L.H. Qiao, Y. Su, P.L. Gao, Z.G. Xie, A postmodification strategy to modulate the photoluminescence of carbon dots from blue to green and red: synthesis and applications, J. Mater. Chem. B 7 (24) (2019) 3840–3845.
[115] B. Lyu, H.-J. Li, F. Xue, L. Sai, B. Gui, D. Qian, et al., Facile, gram-scale and eco-friendly synthesis of multi-color graphene quantum dots by thermal-driven advanced oxidation process, Chem. Eng. J. 388 (2020) 124285.
[116] F.A. Permatasari, H. Fukazawa, T. Ogi, F. Iskandar, K. Okuyama, Design of pyrrolic-N-rich carbon dots with absorption in the first near-infrared window for photothermal therapy, ACS Appl. Nano Mater. 1 (5) (2018) 2368–2375.
[117] D. Gao, Y. Zhang, A. Liu, Y. Zhu, S. Chen, D. Wei, et al., Photoluminescence-tunable carbon dots from synergy effect of sulfur doping and water engineering, Chem. Eng. J. 388 (2020) 124199.
[118] Y. Liu, W. Duan, W. Song, J. Liu, C. Ren, J. Wu, et al., Red emission B, N, S-co-Doped carbon dots for colorimetric and fluorescent dual mode detection of Fe3+ ions in complex biological fluids and living cells, ACS Appl. Mater. Interfaces 9 (14) (2017) 12663–12672.
[119] Y. Fan, X. Guo, Y. Zhang, Y. Lv, J. Zhao, X. Liu, Efficient and stable red emissive carbon nanoparticles with a hollow sphere structure for white light-emitting diodes, ACS Appl. Mater. Interfaces 8 (46) (2016) 31863–31870.
[120] P. Khare, A. Bhati, S.R. Anand, Gunture, S.K. Sonkar, Brightly fluorescent zinc-doped red-emitting carbon dots for the sunlight-induced photoreduction of Cr(VI) to Cr(III), ACS Omega 3 (5) (2018) 5187–5194.
[121] S. Yang, X. Sun, Z. Wang, X. Wang, G. Guo, Q. Pu, Anomalous enhancement of fluorescence of carbon dots through lanthanum doping and potential application in intracellular imaging of ferric ion, Nano Res 11 (3) (2018) 1369–1378.
[122] F. Yuan, L. Ding, Y. Li, X. Li, L. Fan, S. Zhou, et al., Multicolor fluorescent graphene quantum dots colorimetrically responsive to all-pH and a wide temperature range, Nanoscale 7 (27) (2015) 11727–11733.
[123] J.K. Ren, J.B. Sun, X.M. Sun, R. Song, Z. Xie, S.Y. Zhou, Precisely controlled up/down-conversion liquid and solid state photoluminescence of carbon dots, Adv. Opt. Mat. 6 (14) (2018) 1800115.
[124] J. He, Y. He, Y. Chen, B. Lei, J. Zhuang, Y. Xiao, et al., Solid-state carbon dots with red fluorescence and efficient construction of dual-fluorescence morphologies, Small 13 (26) (2017) 1700075.
[125] Y. Zhang, J. Xiao, P. Zhuo, H. Yin, Y. Fan, X. Liu, et al., Carbon dots exhibiting concentration-dependent full-visible-spectrum emission for light-emitting diode applications, ACS Appl. Mater. Interfaces 11 (49) (2019) 46054–46061.

[126] T. Meng, T. Yuan, X. Li, Y. Li, L. Fan, S. Yang, Ultrabroad-band, red sufficient, solid white emission from carbon quantum dot aggregation for single component warm white light emitting diodes with a 91 high color rendering index, Chem. Commun. 55 (46) (2019) 6531–6534.
[127] Z. Han, Y. Ni, J. Ren, W. Zhang, Y. Wang, Z. Xie, et al., Highly efficient and ultra-narrow bandwidth orange emissive carbon dots for microcavity lasers, Nanoscale 11 (24) (2019) 11577–11583.
[128] F. Yuan, Y.-K. Wang, G. Sharma, Y. Dong, X. Zheng, P. Li, et al., Bright high-colour-purity deep-blue carbon dot light-emitting diodes via efficient edge amination, Nat. Photon. 14 (3) (2019) 171–176.
[129] H. Ding, X. Zhou, B. Qin, Z. Zhou, Y. Zhao, Highly fluorescent near-infrared emitting carbon dots derived from lemon juice and its bioimaging application, J. Lumin. 211 (2019) 298–304.
[130] S. Sun, L. Zhang, K. Jiang, A. Wu, H. Lin, Toward high-efficient red emissive carbon dots: facile preparation, unique properties, and applications as multifunctional theranostic agents, Chem. Mater. 28 (23) (2016) 8659–8668.
[131] B.Y. Wang, J. Li, Z.Y. Tang, B. Yang, S.Y. Lu, Near-infrared emissive carbon dots with 33.96% emission in aqueous solution for cellular sensing and light-emitting diodes, Sci. Bull. 64 (17) (2019) 1285–1292.
[132] H.M. Xiong, Y. Xu, Q.G. Ren, Y.Y. Xia, Stable Aqueous ZnO@polymer core-shell nanoparticles with tunable photoluminescence and their application in cell imaging, J. Am. Chem. Soc. 130 (2008) 7522–7523.
[133] X.X. Shi, Y.L. Hu, H.M. Meng, J. Yang, L.B. Qu, X.B. Zhang, et al., Red emissive carbon dots with dual targetability for imaging polarity in living cells, Sensor. Actuator. B Chem. 306 (2020) 7.
[134] X.W. Hua, Y.W. Bao, J. Zeng, F.G. Wu, Nucleolus-targeted red emissive carbon dots with polarity-sensitive and excitation-independent fluorescence emission: high-resolution cell imaging and in vivo tracking, ACS Appl. Mater. Interfaces 11 (36) (2019) 32647–32658.
[135] D. Li, C. Liang, E.V. Ushakova, M. Sun, X. Huang, X. Zhang, et al., Thermally activated upconversion near-infrared photoluminescence from carbon dots synthesized via microwave assisted exfoliation, Small 15 (50) (2019) 1905050.
[136] G.Y. Xu, X. Bao, J.Q. Chen, B.H. Zhang, D. Li, D. Zhou, et al., In vivo tumor photoacoustic imaging and photothermal therapy based on supra-(carbon nanodots), Adv. Healthcare Mater. 8 (2) (2019) 1800995.
[137] F. Wu, H. Su, Y. Cai, W.-K. Wong, W. Jiang, X. Zhu, Porphyrin-implanted carbon nanodots for photoacoustic imaging and in vivo breast cancer ablation, ACS Appl. Nano Mater 1 (1) (2018) 110–117.
[138] X. Sun, Y. Lei, Fluorescent carbon dots and their sensing applications, TrAC Trends Anal. Chem. (Reference Ed.) 89 (2017) 163–180.
[139] H. Feng, Z. Qian, Functional carbon quantum dots: a versatile platform for chemosensing and biosensing, Chem. Rec. 18 (5) (2018) 491–505.
[140] C. Liu, D. Ning, C. Zhang, Z. Liu, R. Zhang, J. Zhao, et al., Dual-colored carbon dot ratiometric fluorescent test paper based on a specific spectral energy transfer for semiquantitative assay of copper ions, ACS Appl. Mater. Interfaces 9 (22) (2017) 18897–18903.
[141] J. Xia, S. Chen, G.Y. Zou, Y.L. Yu, J.H. Wang, Synthesis of highly stable red-emissive carbon polymer dots by modulated polymerization: from the mechanism to application in intracellular pH imaging, Nanoscale 10 (47) (2018) 22484–22492.
[142] W. Song, W. Duan, Y. Liu, Z. Ye, Y. Chen, H. Chen, et al., Ratiometric detection of intracellular lysine and pH with one-pot synthesized dual emissive carbon dots, Anal. Chem. 89 (24) (2017) 13626–13633.
[143] Y. Hu, Z. Yang, X. Lu, J. Guo, R. Cheng, L. Zhu, et al., Facile synthesis of red dual-emissive carbon dots for ratiometric fluorescence sensing and cellular imaging, Nanoscale 12 (9) (2020) 5494–5500.
[144] H. Li, D. Su, H. Gao, X. Yan, D. Kong, R. Jin, et al., Design of red emissive carbon dots: robust performance for analytical applications in pesticide monitoring, Anal. Chem. 92 (4) (2020) 3198–3205.
[145] Y.J. Ju, N. Li, S.G. Liu, J.Y. Liang, X. Gao, Y.Z. Fan, et al., Proton-controlled synthesis of red-emitting carbon dots and application for hematin detection in human erythrocytes, Anal. Bioanal. Chem. 411 (6) (2019) 1159–1167.
[146] X.Q. Liu, T. Wang, W.J. Wang, Z.P. Zhou, Y.S. Yan, A tailored molecular imprinting ratiometric fluorescent sensor based on red/blue carbon dots for ultrasensitive tetracycline detection, J. Ind. Eng. Chem. 72 (2019) 100–106.
[147] F. Du, Z. Cheng, Z. Lai, G. Ruan, C. Zhao, Red-emissive nitrogen doped carbon quantum dots for highly selective and sensitive fluorescence detection of the alachlor herbicide in soil samples, New J. Chem. 43 (47) (2019) 18695–18701.
[148] Y. Chen, X. Sun, X. Wang, W. Pan, G. Yu, J. Wang, Carbon dots with red emission for bioimaging of fungal cells and detecting Hg2+ and ziram in aqueous solution, Spectrochim. Acta Mol. Biomol. Spectrosc. 233 (2020) 118230.
[149] Y. Wen, Q. Jia, F. Nan, X. Zheng, W. Liu, J. Wu, et al., Pheophytin derived near-infrared-light responsive carbon dot assembly as a new phototheranotic agent for bioimaging and photodynamic therapy, Chem. Asian J. 14 (12) (2019) 2162–2168.
[150] Q. Jia, X. Zheng, J. Ge, W. Liu, H. Ren, S. Chen, et al., Synthesis of carbon dots from Hypocrella bambusae for bimodel fluorescence/photoacoustic imaging-guided synergistic photodynamic/photothermal therapy of cancer, J. Colloid Interface Sci. 526 (2018) 302–311.
[151] Q. Jia, J. Ge, W. Liu, L. Guo, X. Zheng, S. Chen, et al., Self-assembled carbon dot nanosphere: a robust, near-infrared light-responsive, and vein injectable photosensitizer, Adv. Healthcare Mater. 6 (12) (2017) 1601419.
[152] Y. Su, S.Y. Lu, P.L. Gao, M. Zheng, Z.G. Xie, BODIPY@carbon dot nanocomposites for enhanced photodynamic activity, Mater. Chem. Front. 3 (9) (2019) 1747–1753.
[153] Z.A.I. Mazrad, K. Lee, A. Chae, I. In, H. Lee, S.Y. Park, Progress in internal/external stimuli responsive fluorescent carbon nanoparticles for theranostic and sensing applications, J. Mater. Chem. B 6 (8) (2018) 1149–1178.